ADVANCES IN ATOMIC, MOLECULAR, AND OPTICAL PHYSICS, VOL. 35

FEMTOSECOND SPECTROSCOPY OF MOLECULES AND CLUSTERS[1]

T. BAUMERT and G. GERBER

Physikalisches Institut der Universität, Am Hubland, D-97074 Würzburg, Germany

I. Introduction

Many gases in nature are diatomics. The simple way of thinking about a diatomic molecule is the imagination of two spheres connected by a rigid rod, symbolizing the chemical bond. This bond is of course not rigid, since the atoms are vibrating against each other. This dynamical view on molecules is usually not treated in quantum mechanical textbooks because the time-dependent part of the Schrödinger equation is separated and only the time-independent Schrödinger equation is solved, whose solutions are of course time independent and do not describe the dynamical aspects of molecules.

[1]Work has been performed at the University of Freiburg, Germany.

ISBN 0-12-003835-8

By coherent coupling of the vibrational states of a molecule a vibrational wavepacket is formed. The different evolution of the phases of these vibrational eigenfunctions leads to a motion of the wavepacket that resembles the classical oscillatory motion. This was realized by Erwin Schrödinger himself (Schrödinger, 1926) shortly after he had published his Schrödinger equation. In that work he constructed a wavepacket in a harmonic oscillator potential and showed that this wavepacket moves like a point mass according to the laws of classical mechanics.

With the development of ultrafast laser sources with their inherent spectral width it has become a standard technique to couple coherently quantum mechanical eigenstates. The observation of Rydberg wavepackets in atoms (ten Widle *et al.*, 1989; Yeazall *et al.*, 1990), showing the classical Kepler orbits of the electron around the nucleus (Averbukh and Perelman, 1989), and the observation of vibrational wavepackets in molecules (Bowman *et al.*, 1989; Fragnito *et al.*, 1989; Baumert *et al.*, 1991a) are prominent examples.

Besides the beauty of looking at a quantum mechancial system from a classical point of view these time-resolved techniques have influenced many areas in physics, chemistry, biology, and technology (for examples see *Ultrafast Phenomena IX*, 1994). Many formerly unfeasible experiments can now be performed in the time domain, and often the results of time domain experiments are interpreted more directly than results obtained in the frequency domain. Examples from molecular and cluster physics will be discussed in this chapter.

In the molecular physics section we first discuss the evolution of a vibrational wavepacket in a double minimum potential well. Second, we will focus on the dynamics of multiphoton ionization (MPI) in a diatomic, and we will see how the unexpected results give new input into the challenging field of controlling chemical reactions by means of time-resolved laser techniques. As high laser intensities are achieved in focused ultrashort light pulses, their interaction with molecules is of particular interest and will be treated next. For all these experiments we have chosen the Na_2 molecule as a model system, as there is a wealth of spectroscopic and theoretical information available, which facilitates the interpretation of the time domain results considerably.

In the cluster section of this chapter we report the first experiments in cluster physics employing ultrashort laser pulses to time-resolved studies of cluster ionization and fragmentation processes. Clusters and in particular metal clusters have been the fascinating subject of many experimental and theoretical studies. Clusters form the link between solid-state physics and molecular physics. Metal clusters exhibit distinct features ranging from molecular properties seen in small particles to the solid state like behavior of larger aggregates. Studies of cluster properties like geometric structures, the evolution of the electronic states from localized to delocalized in nature, and the real-time dynamics of ionization and fragmentation have not yet

been performed in detail as a function of cluster size. Alkali clusters are attractive species to be studied experimentally and theoretically, because there is only one valence electron per atom. We will describe cluster-size-dependent studies of physical properties of sodium clusters such as absorption resonances, lifetimes, and decay channels using tunable femtosecond light pulses in resonance-enhanced multiphoton ionization (REMPI) of the *neutral* cluster size under investigation. Two-photon ionization spectroscopy failed in nanosecond-laser experiments due to the ultrafast decay of the studied neutral clusters. The other metal cluster system we will report on is the mercury clusters, Hg_n. In experiments with single femtosecond laser pulses prompt formation of singly and doubly charged clusters are observed up to $n \approx 60$. In pump-probe experiments the transient multiphoton ionization spectra show a "short"-time wavepacket dynamics, which is identical for all observed singly and doubly charged mercury clusters. The "long"-time fragmentation and recombination dynamics, however, indicating a cage effect behavior, is different for the individual clusters.

II. Experimental Setup

The time-resolved femtosecond laser studies in molecular/cluster physics are performed with a combination of experimental techniques: A supersonic (seeded) molecular/cluster beam provides the molecules/clusters in a collision-free environment and restricts the set of initial states mainly to $v'' = 0, J''$. Time-of-flight (TOF) mass spectrometry is used to determine the mass of the ions, the released kinetic energy of the ionic fragments, and the energy distribution of the ejected electrons. Because the ion and electron detection angles are fixed, the ion and electron angular distributions can be studied by rotating the laser polarization. We are thus able to determine the final continuum states. The collinear femtosecond pump–probe techniques are used to induce and to probe molecular/cluster transitions, to resolve the interactions, and to display the evolution of coherences and populations in real time.

The schematic experimental arrangements of the molecular beam apparatus and the ion and electron TOF spectrometers are shown in Fig. 1. In the following section we will describe the experimental setup in detail.

A. Molecular/Cluster Beam and TOF Spectrometer

The supersonic sodium molecular/cluster beam is produced by a coexpansion of sodium vapor (50–100 mbar) with the inert carrier gas argon (1–8 bar) through a small orifice about 100 μm in diameter. In order to achieve this vapor pressure the oven is usually operated at 1000 K with nozzle temperatures about 50 K higher. This technique provides efficiently

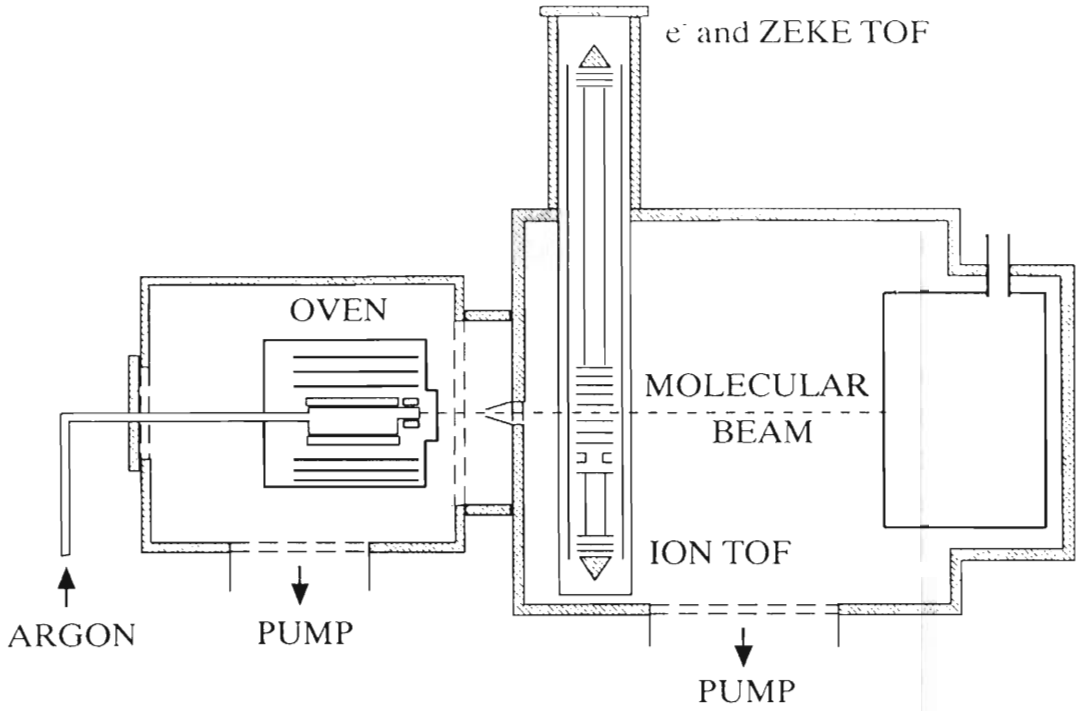

FIG. 1. Sectional drawing of the molecular/cluster beam apparatus and the two different designed TOF spectrometers. The femtosecond lasers (not shown), the molecular/cluster beam axis, and the spectrometer axis are mutually perpendicular to each other.

cooled sodium molecules/clusters. We have measured a vibrational temperature of about 50 K for Na_3 and a rotational temperature of about 15 K for Na_2. With a similar setup and a carrier gas pressure of 10 bar, vibrational temperatures as low as 25 K for Na_3 have been reported (Broyer *et al.*, 1987). To produce mercury clusters, Hg_n, with this technique, the necessary oven temperatures are much lower.

The laser–molecular beam interaction region is placed between parallel ring-shaped plates so that the formed ions and electrons can be detected in opposite directions by two differently designed TOF spectrometers. Both TOF spectrometers are perpendicular to the laser beam axis and the molecular beam axis. Extracting the ions with a low electric field (5–10 V/cm), the ion time of flight depends on the mass and on the projection of the initial fragment velocity onto the spectrometer axis. Thus, by knowing the extraction field, the measured time-of-flight spectrum is transformed into a velocity spectrum, from which upper bounds of the fragment kinetic energy are determined. This experimental technique is widely known (Wiley and McLaren, 1955; Ogorzalek Loo *et al.*, 1988; Baumert *et al.*, 1993a). The mass resolution $m/\Delta m$ of our ion TOF spectrometer is about 100 and is sufficient to study molecules and small metal cluster systems. The energy calibration of the electron TOF spectrometer is based upon several one- and two-photon resonance-enhanced ionizing transitions in atomic sodium, leading to electrons with well-defined kinetic energy. The energy resolution of the electron TOF spectrometer is 25 to 80 meV in the range of 0.1 to 3 eV. With our ZEKE (zero kinetic energy) photoelectron spectrometer, built according

to the design of Müller-Dethlefs and Schlag (Müller-Dethlefs *et al.*, 1984), we achieve an electron energy resolution of 0.1 meV (or about 1 cm^{-1}).

B. The Femtosecond Laser Systems

Femtosecond light pulses are generated in two different home-built laser systems. Independently tunable femtosecond pulses down to 50 fs time duration and up to 50 μJ energy are generated in the laser system shown in Fig. 2. The tunability of our present system covers the near UV, the complete visible range, and the near IR. The output pulses either of a colliding-pulse mode-locked (CPM) ring dye laser (see below) or of a Ti:sapphire oscillator (see below) are amplified in a bow-tie amplifier, which is pumped by an excimer laser at 308 nm, pulse compressed, and focused into a cell containing methanol to generate a white light continuum. Further amplification schemes for ultrashort dye laser pulses are reviewed in Knox (1988), Simon (1989), and Heist *et al.* (1990). Pump and probe pulses at specific wavelengths are selected from the white light continuum with a grating, which can also be used to compensate for group velocity dispersion in the subsequent amplification stages. Using adjustable slits for wavelength selection, the bandwidth of the pulses can be chosen depending upon the requirements of the experiment (Noordam *et al.*, 1991). Pump and probe pulses are amplified again in two additional bow-tie amplifiers. Additional wavelength conversion methods like frequency doubling are used to generate tunable ultrashort UV–laser pulses. The pump and probe laser beams are recombined collinearly and focused into the interaction region. A Michelson arrangement is used to delay the probe laser pulse relative to the pump laser pulse.

1. The CPM Oscillator

In our initial setup we decided to use a colliding pulse mode-locked ring dye laser (CPM) (Fork *et al.*, 1981) as a source of the femtosecond laser pulses, because of the ease of getting into the sub-100-fs regime and because of the reliability of this kind of passively mode-locked laser in terms of pulse stability. This choice implied a nanosecond laser for pumping the amplification stages. We decided on an excimer laser (Lambda Physik LPX 120i) with a 200-Hz repetition rate and a maximum of 200 mJ pulse energy in a 17-ns pulse. This laser is a compromise between the low repetition (high pulse energy) Nd:YAG laser systems and the high repetition rate (low energy) copper vapor laser systems. Because of the wavelength of the excimer laser (308 nm, XeCl), pulses even in the blue spectral region — obtained by spectral filtering of the supercontinuum (see above) — can be amplified directly. Building up our CPM laser — indicated at the top of Fig. 2 — we followed the design proposed by Valdmanis and Fork (1986). We

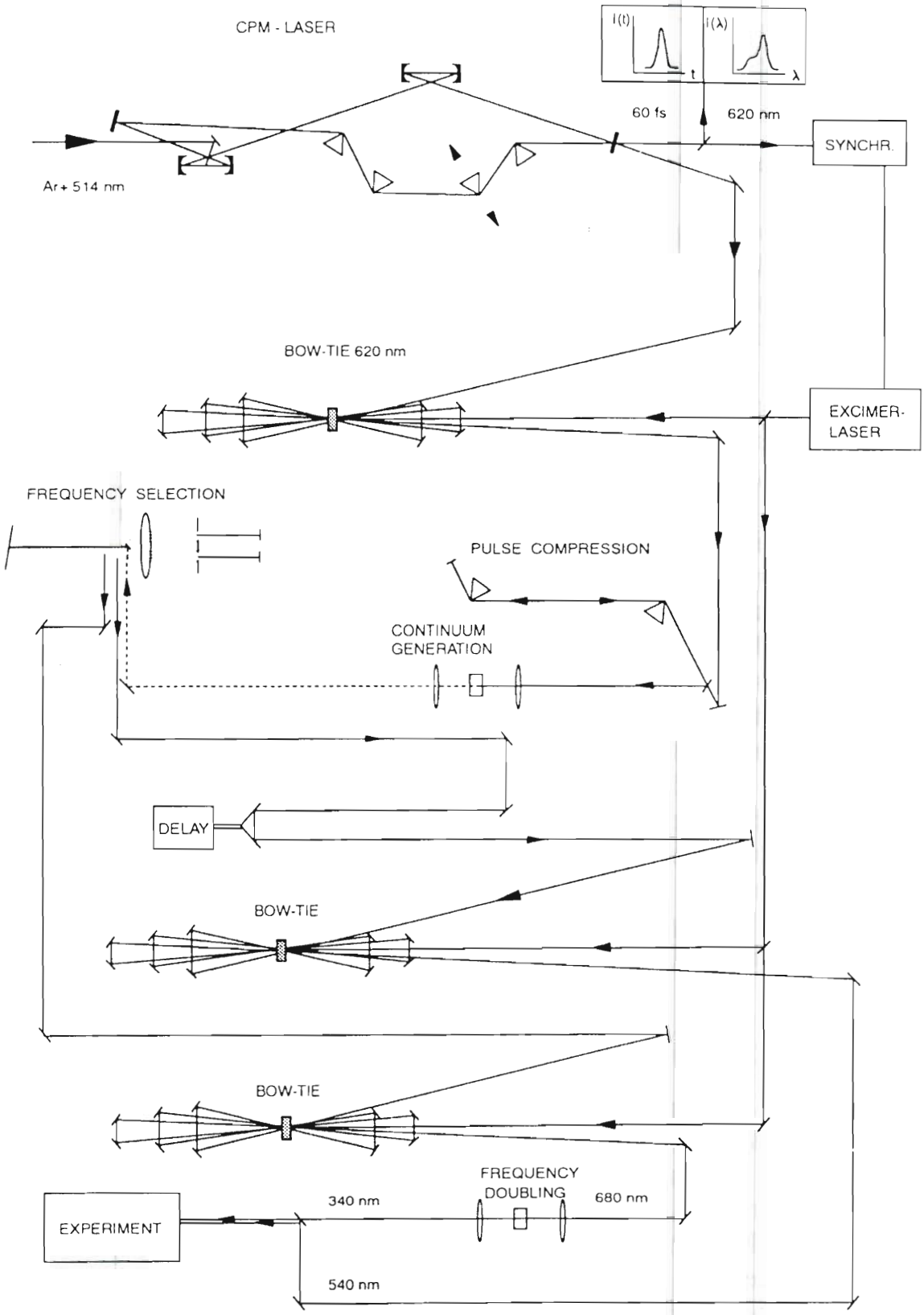

FIG. 2. Femtosecond laser system for independently tunable pump and probe wavelengths.

used broadband dielectric mirrors in the resonator. The folding mirrors have a radius of curvature of 10 cm for the gain and 5 cm for the absorber. The output coupler has a transmission of 3%. Folding angles are 5° (full angle) for the gain folding and 10° for the absorber. They are determined by mirror dimensions. We decided on a 4-m ring resonator, to allow the amplification

of only one pulse out of the pulse train of the CPM, during the 17-ns pulse duration of the excimer laser. We use Rhodamine 6G (2.3×10^{-3} molarity dissolved in ethylene glycol) for the gain and DODCI (dissolved in ethylene glycol) for the absorber. The concentration of the DODCI is determined by the desired wavelength and varies in the range of 10^{-4} to 10^{-5} molarity. Standard coherent nozzles are used for the gain and the absorber jets. Compensation of the intracavity group velocity dispersion is accomplished with the standard four-prism design. The fused silica prisms have a distance of 38 cm. The 514.5-nm light of the Ar^+ laser is focused down by a 5-cm folding mirror. With 4 W pump power we obtain pulses of 60 fs sech^2 at a center wavelength of 627 nm. The center wavelength of the CPM dye laser can be shifted in the range 613–630 nm by adjusting the saturable absorber concentration, resulting, however, in a slight increase of the output pulse duration if the laser is shifted to shorter wavelengths. The typical output power for operation in the sub-100-fs regime is 10–15 mW. The pump power dependence of our system is similar to that described in Jacobovitz *et al.* (1986). One output of the ring laser is used to monitor the spectral and temporal behavior of the laser and to derive a synchronization signal for the excimer laser. The other output is used for amplification. The spectral distribution is measured on line with an optical multichannel analyzer (OMA). The pulse duration is determined by the autocorrelation technique using collinear and anticollinear second harmonic generation in a 1-mm KDP crystal and assuming a sech^2 pulse shape (Ippen and Shank, 1977). We built the resonator using ABCD resonator calculations (Kogelnik and Li, 1966; Rigrod, 1965; Li, 1982). Having the boundary conditions of 4 m resonator length, spacing of the saturable absorber jet and gain jet of one-quarter of the total round trip, and folding angles of 5° and 10°, we computed the common stability region of tangential and sagittal stability points by varying the absorber folding distance d_1 and the gain folding distance d_2. For these stability points we calculated the location and the spot size of the tangential and sagittal beam waists. Knowing the spot sizes one can perform an *s*-parameter analysis (New, 1974). This information is not very useful in CPM lasers as the dispersive pulse shaping mechanism is more dominant than pulse shaping by saturable gain and saturable absorption for production of the ultrashort laser pulses. This can be seen because the shortest pulses are often not obtained when the saturable absorber is placed into the focus (largest *s*-parameter) but a few 100 μm away from the focus. Knowing the location of the beam waists is useful information because straightforward alignment procedures can be derived from this by simply applying Descartes' formula for sagittal and tangential image points. We applied this concept to a 1.9-m CPM resonator and to the 4-m resonator and found in both cases that the calculated alignment leads to stable ring dye laser operation. In the 4-m resonator geometry we took the stability point $d_1 = 10.55$ cm and $d_2 = 5.25$ cm for the alignment. In the gain folding we got for the location l_s and l_t of the beam waist $l_s = 5.45$ cm and

$l_t = 5.43$ cm in the direction toward the saturable absorber folding. In the absorber folding we got $l_s = 2.53$ cm and $l_t = 2.53$ cm in the direction toward the output coupler. To align the gain folding distances we used the fluorescence light from the pump spot of the Ar^+ laser on the gain jet, and to adjust the absorber folding we used a slit to align the distance of the two mirrors. The threshold pump power for cw operation of the ring was then 0.9 W.

2. *The Ti:Sapphire Oscillator*

We have built an amplified Ti:sapphire laser system based on the chirped pulse amplification (CPA) technique (Strickland and Mourou, 1985). While dye amplifier systems are limited to average power outputs on the order of 10 mW, up-to-date solid-state systems can produce more than 2 W of average power with peak powers of 14 GW (Squier *et al.*, 1993). For the experiments with mercury clusters we used the Ti:sapphire oscillator described below. This Ti:sapphire laser produces 20- to 70-fs light pulses in the wavelength range 700 to 810 nm. Using again the excimer pumped bow-tie amplifiers pulse energies of the order of several 10 μJ are obtained. The setup of this laser system is depicted in Fig. 3. Contemporary Ti:sapphire laser designs are able to produce pulses as short as 11 fs (Asaki *et al.*, 1993; Stingl *et al.*, 1994). Pulse durations as low as 8.2 fs were reported (Stingl, 1994).

Our Ti:sapphire oscillator is shown in the upper part of Fig. 3. The folding mirrors have a radius of curvature of 10 cm. The distance from the left folding mirror to the end mirror is about 80 cm and the distance from the right folding mirror to the output coupler is also 80 cm. The prisms, made of LaKL21, are spaced by 33 cm in order to minimize cubic phase distortions. The 8-mm-long Ti:sapphire rod has Brewster end faces and is doped with 0.1% Titan. Again we performed and ABCD matrix analysis of the resonator: the astigmatism of the laser rod is compensated for a folding angle of 19.25°; stable operation is then achieved in a region from 4.86 to 5.16 cm (distance from folding mirrors to the Brewster end faces of the laser rod). The laser rod is pumped by an all-lines Ar^+ laser focused with a 10-cm focusing lens. Typical pump powers are in the range from 4 to 5 W, resulting in an average output power of 50 to 400 mW of the femtosecond oscillator.

C. The Pump–Probe Delay Line

For the one-color pump–probe experiments we used a Michelson arrangement with a 50% beam splitter to delay the probe laser pulse relative to the pump laser pulse. A computer-controlled stepper-motor-driven linear preci-

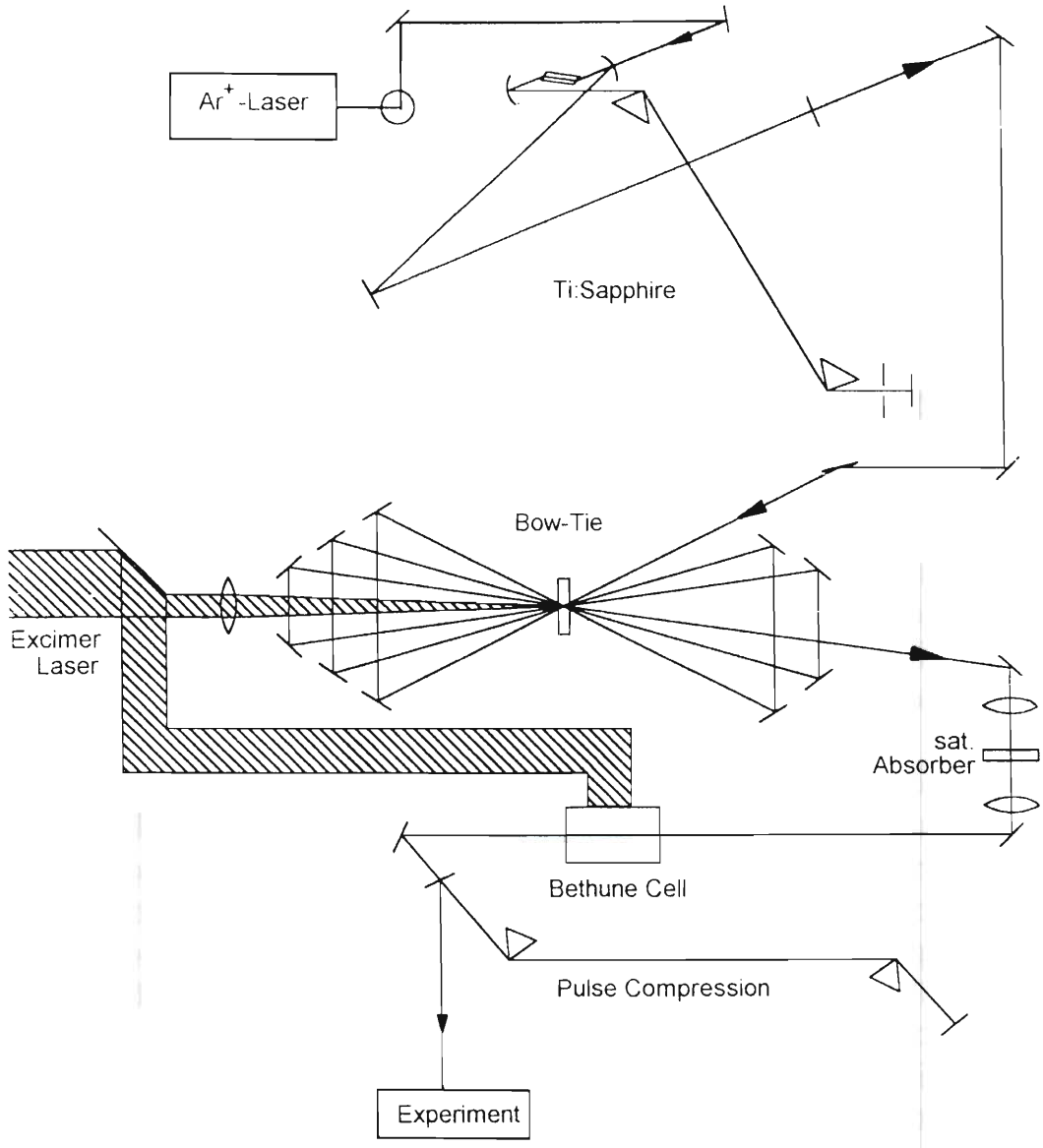

FIG. 3. Schematic setup of the Ti:sapphire femtosecond laser system. In the upper figure the Ti:sapphire oscillator is shown. The slit is used to tune the laser wavelength.

sion actuator with a 0.05-μm feed in one arm of the interferometer sets the time delay. The pulses are recombined collinearly. Thus we obtain identical pulses for the pump and the probe lasers. The pulses are identical in polarization, wavelength, energy, and duration. The advantage of one-color pump–probe experiments is that the dynamics of multiphoton ionization studied with femtosecond laser pulses can directly be compared with one-color nanosecond laser multiphoton experiments. Identical pump and probe laser pulses are crucial for this comparison. A further advantage is that in this case symmetric spectra are always obtained with respect to zero delay time. With an accurate determination of zero delay time, phase information can be derived from the observed wavepacket motion. The disadvantage of a Michelson pump–probe arrangement is the loss of half of the pulse energy at the beam splitter. The same actuator has also been used

in two-color pump–probe experiments. A typical two-color pump–probe femtosecond laser system is depicted in Fig. 2.

D. Data Acquisition

The data for the Na^+, Na_2^+, and Na_3^+ transients in the one-color pump–probe experiments were taken in the following way: the MCP (multichannel plates) signal of the TOF spectrometer is fed into a boxcar integrator (SR 255). The boxcar is triggered by a laser reflex monitored by a fast photodiode. The gate of the boxcar is set to the ionic mass to be measured. Note that in a TOF spectrometer the time of flight of an ion is proportional to the square root of the mass of this ion. The integration of the boxcar averager is set to 300 or 1000 laser shots. With a given repetition rate of the amplified pulses the feed of the stepper motor is set such that during an integration over 300 or 1000 laser shots a pump–probe delay time of 20 fs is scanned. The reason for the choice of such an averaging interval (AI) is that AI has to be greater than 1 fs to get rid of interferometric structures from overlapping pump and probe pulses. The same condition is applied to collinear intensity autocorrelation measurements. On the other hand AI has to be much smaller than the pulse duration in order not to lose time resolution. In particular for a fast Fourier transformation (FFT) the sampling interval of the FFT (that corresponds to AI) should be smaller than half of the pulse width to avoid aliasing effects in the FFT spectra. So in our (one-color pump–probe) transient Na^+, Na_2^+, and Na_3^+ spectra each data point corresponds to a pump–probe delay time interval of 20 fs and each of these intervals is averaged over 300 or 1000 laser shots.

The laser intensities in all experiments were monitored with calibrated photodiodes and an additional boxcar averager. The data for the cluster experiments were taken with a CAMAC transient recorder (Transiac 2001 AS, DSP) and averager (4101, DSP).

III. Results and Discussion of Experiments in Molecular Physics

A. Vibrational Wave-Packet Motion in the $2\,^1\Sigma_u^+$ Double Minimum State of Na_2

In this section we will first discuss the propagation of a wavepacket in a double minimum potential well. Then the experimental preparation and detection of a vibrational wavepacket on such an excited electronic surface are considered. Furthermore we will show that frequency spectroscopy can be performed in the time domain as well.

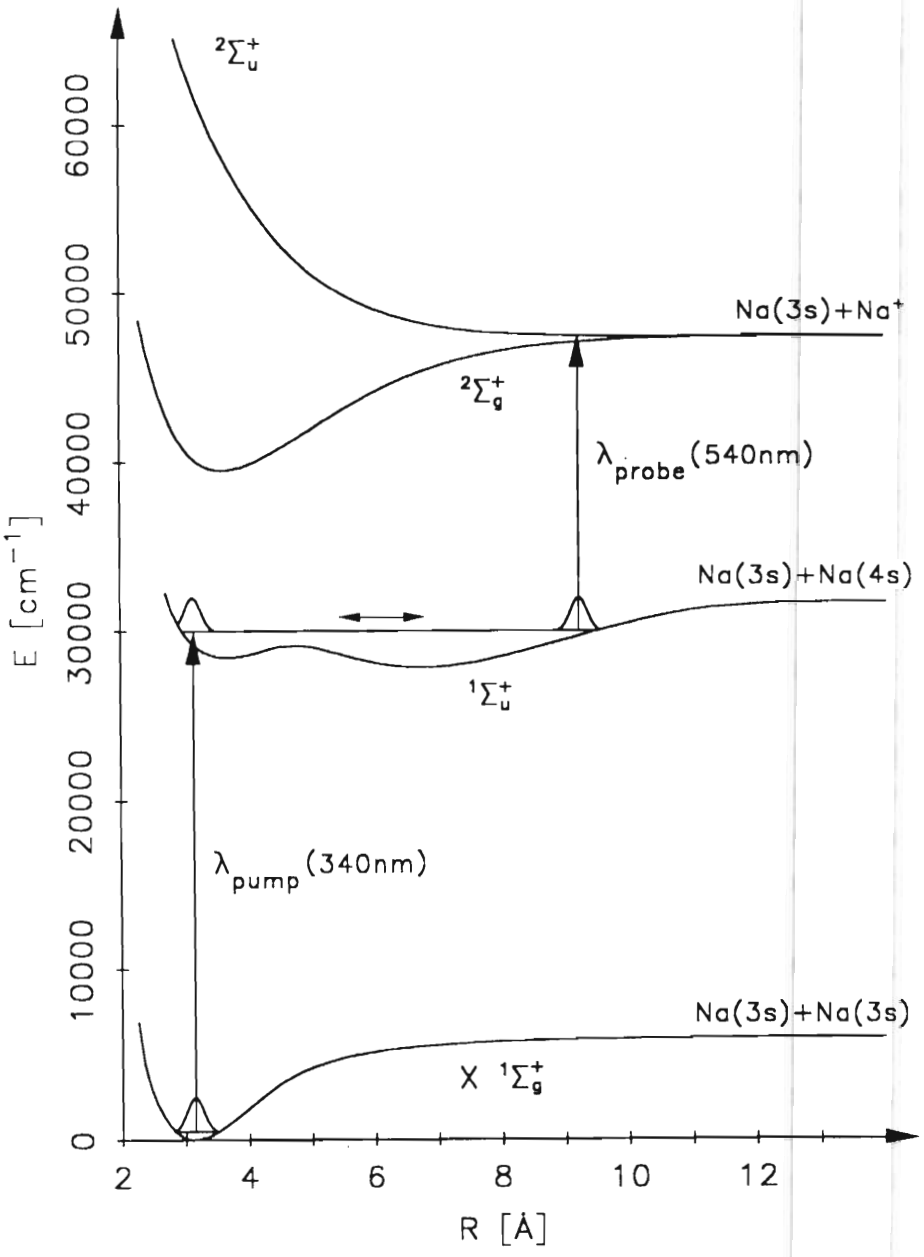

FIG. 4. Potential energy surfaces relevant for the pump–probe experiment on the $2\,^1\Sigma_u^+$ double minimum state of the Na_2. The pump laser prepares a vibrational wavepacket at the inner turning point above the barrier. The probe laser transfers this wavepacket at the outer turning point onto the repulsive $^2\Sigma_u^+$ ionic state of the Na_2. Measuring the Na^+ signal as a function of pump–probe delay therefore resembles the wavepacket dynamics in the double minimum state.

The double minimum structure of the $2\,^1\Sigma_u^+$ state of Na_2 (see Fig. 4) is formed by the avoided crossing of two adiabatic potential curves. One has mainly Rydberg character and the other has a substantial ionic character at large internuclear distances. The inner potential minimum is at an internuclear distance of 3.688 Å and at an energy of 28454.56 cm^{-1}; the outer potential minimum is located at 6.739 Å with an energy of 27879.40 cm^{-1} (Cooper *et al.*, 1984; Vergès *et al.*, 1984). The barrier is at 4.716 Å with an energy of 29132 cm^{-1}. The top of the barrier corresponds

to an excitation wavelength of 344.2 nm relative to the $X\,^1\Sigma_g^+$ ($v'' = 0$) state. The $2\,^1\Sigma_u^+$ state was theoretically predicted by Valance and Nguyen Tuan (1982) and confirmed by Jeung (1983). The first experimental observation was reported by Cooper *et al.* (1984) and Vergès *et al.* (1984). They employed Fourier transform spectroscopy of the laser-induced infrared fluorescence. Experiments involving the two-photon ionization (TPI) technique were performed by Delacrétaz and Wöste (1985) and by Haugstätter *et al.* (1988).

By using time-dependent perturbation theory and its implementations into time-dependent molecular physics (Kulander and Heller, 1978; Engel, 1991a) we have calculated the propagation of a wavepacket created by the coherent superposition of vibrational eigenstates at the inner turning point of the $2\,^1\Sigma_u^+$ state with an 80-fs excitation pulse. Note, that no quantum calculations are needed if the only interest is the average classical oscillation period T as T is simply given by $T = 1/\Delta\nu$, where $\Delta\nu$ is the average vibrational spacing in Hertz.

The results of the quantum calculations are displayed in Fig. 5. There is a strong dependence of the wavepacket dynamics with respect to its energy or equivalently to the wavelength of the exciting laser pulse. At $\lambda = 347$ nm the wavepacket is excited below the barrier, and therefore only motion within the inner well is possible. Centering the energy of the wavepacket at the barrier ($\lambda = 344.2$ nm) the wavepacket splits into a transmitted and reflected part as is expected from basic quantum mechanics. At an excitation energy of $\lambda = 341.5$ nm the wavepacket is already above the barrier. At $\lambda = 335$ nm the wavepacket is far above the barrier, and the dynamics represents nicely the classical motion of a point mass in this potential well. Transient electron spectra reflecting wavepacket motion in this $2\,^1\Sigma_u^+$ state were calculated by Meier and Engel (1994a). They used an excitation scheme similar to that described below.

In order to prepare a wavepacket above the barrier experimentally, we excited the molecule with a short pump pulse at $\lambda = 340$ nm. The wavepacket is created at the inner turning point of the $2\,^1\Sigma_u^+$ state, as we start from $v'' = 0$ in the narrow $X\,^1\Sigma_g^+$ state (see Fig. 4). In general, classical transition regions are determined by the Mulliken difference potential analysis (Mulliken, 1971). The application of this analysis to femtosecond pump–probe experiments in molecular physics was discussed by Baumert *et al.* (1991b). Because of the known average vibrational spacings we expected an oscillation period of about 1 ps, as is also seen in the quantum calculations in Fig. 5. The probe laser wavelength is chosen such that only at the outer turning point a transition onto the repulsive $^2\Sigma_u^+$ state of Na_2^+ is possible by energetic and Franck–Condon arguments. The probe laser will therefore form slow atomic Na^+ fragments. Preparing the wavepacket at the inner turning point of the $2\,^1\Sigma_u^+$ state and transferring it into the ionization continuum at the outer turning point, one observes the first signal

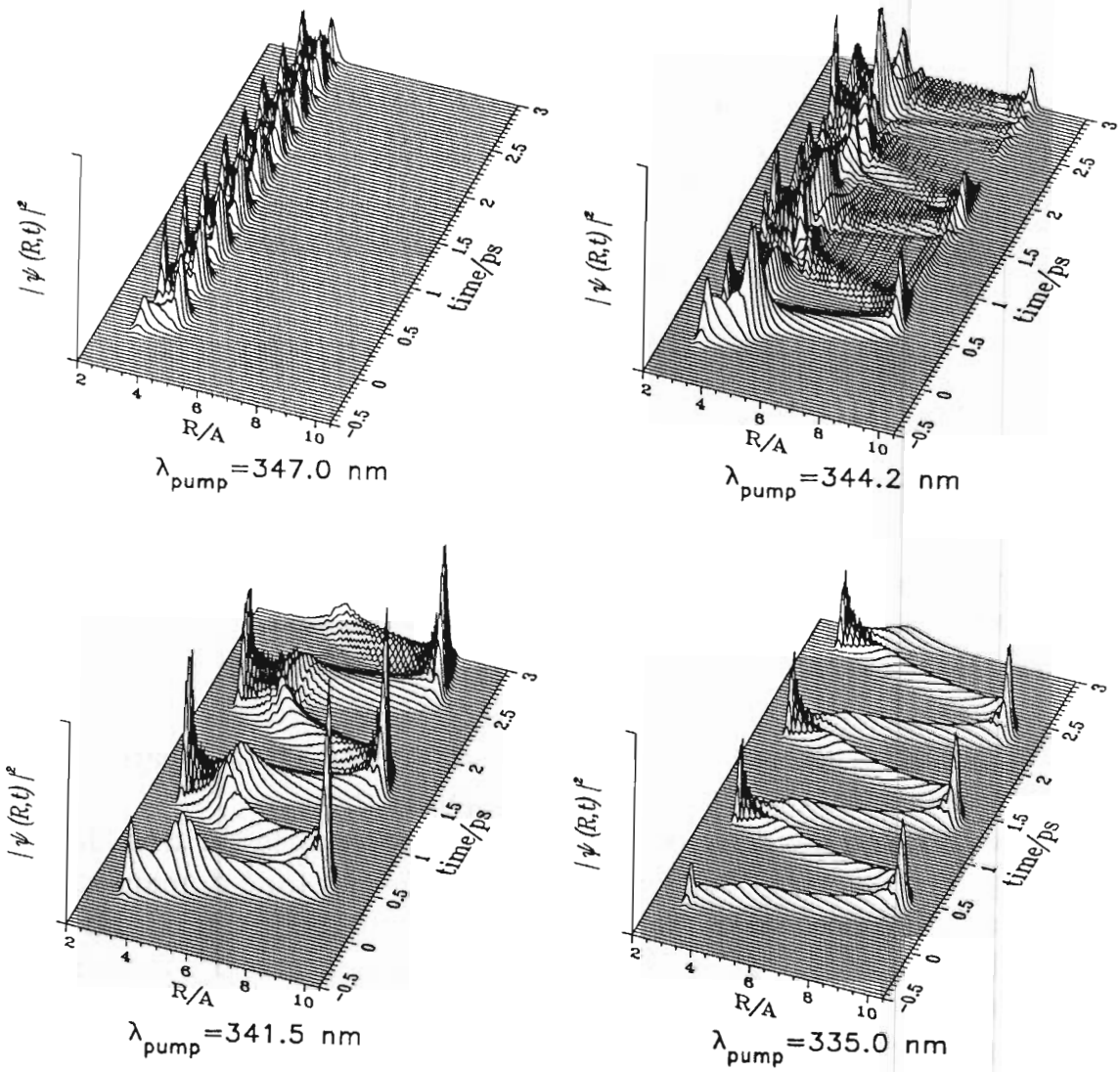

FIG. 5. Dynamical behavior of a wavepacket in the $2\,^1\Sigma_u^+$ double minimum state (Fig. 4) for different excitation energies (see the text): $\lambda_{pump} = 347.0$ nm, below the barrier; $\lambda_{pump} = 344.2$ nm, at the barrier—note that part of the wavepacket is reflected, whereas the other part is transmitted; $\lambda_{pump} = 341.5$ nm, just above the barrier; and $\lambda_{pump} = 335.0$ nm, far above the barrier.

only after half a vibrational period according to the formation of the ionic (Na^+) fragments. Depending on the pump–probe delay the ionic (Na^+) signal is expected to oscillate with a period of about 1 ps. This indeed is what we observed in the experiment. Figure 6 shows the ionic (Na^+) signal versus the pump–probe delay time. The expected 1-ps oscillation is clearly seen. Due to the anharmonicity of the $2\,^1\Sigma_u^+$ potential the vibrational spacings are not constant within the spectral width of the exciting laser pulse. Therefore the amplitude of the observed oscillation decreases with time. This spreading of a vibrational wavepacket takes place in a well-defined way, and the wave packet is restored completely after a certain time, which is known as the recurrence time of a wavepacket. The spreading and recurrence of a vibrational wavepacket motion in the $A\,^1\Sigma_u^+$ state of the sodium dimer was

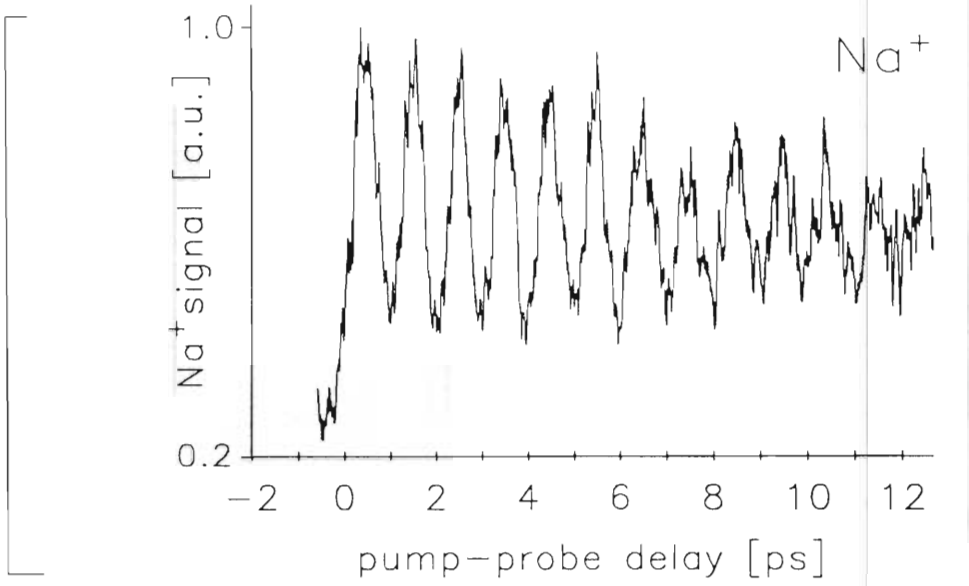

FIG. 6. The measured Na^+ signal as a function of pump–probe delay time shows the expected oscillatory behavior, determined by the $2\,^1\Sigma_u^+$-potential curve.

investigated experimentally (Baumert *et al.*, 1992a). A comparison with quantum calculations is also given in that publication.

Now we turn to the topic of frequency spectroscopy in the time domain. At first glance the terms frequency spectroscopy and time domain seem to be contradictory because of the broad spectral distribution of an ultrashort laser pulse. However, the spectroscopic information can be derived by a Fourier transformation from data taken in the time domain. This has been shown for diatomics and diatomic-like molecules by Zewail's group for the system I_2 (Gruebele *et al.*, 1990) and ICN (Janssen *et al.*, 1990). Although the time domain approach cannot compete with the elaborate techniques of high-resolution spectroscopy for bound systems, for predissociating or dissociative systems this approach might sometimes be the only choice to determine spectroscopic data especially in the transition-state region. Another advantage of the time-resolved method is the ease of distinction between vibrational and rotational spectroscopic information, because energy spacings (e.g., oscillation periods) are different in general by two orders of magnitude. For bound systems the achievable resolution is limited only by the scan length. Using a square window in the Fourier transformation, the theoretical resolution limit for the FWHM is $0.1\,cm^{-1}$ for a scan length of 300 ps. Note that peak positions (frequencies) in such a FFT spectrum can be determined with even higher accuracy.

The correspondence of resolution in the frequency domain and scan length in the time domain is now used in the analysis of our data. The FFT of the transient given in Fig. 6 consists of a frequency distribution centered around $33.4\,cm^{-1}$ (corresponding to 1 ps), where the individual energy spacings of the vibrational levels the wavepacket is composed of are not

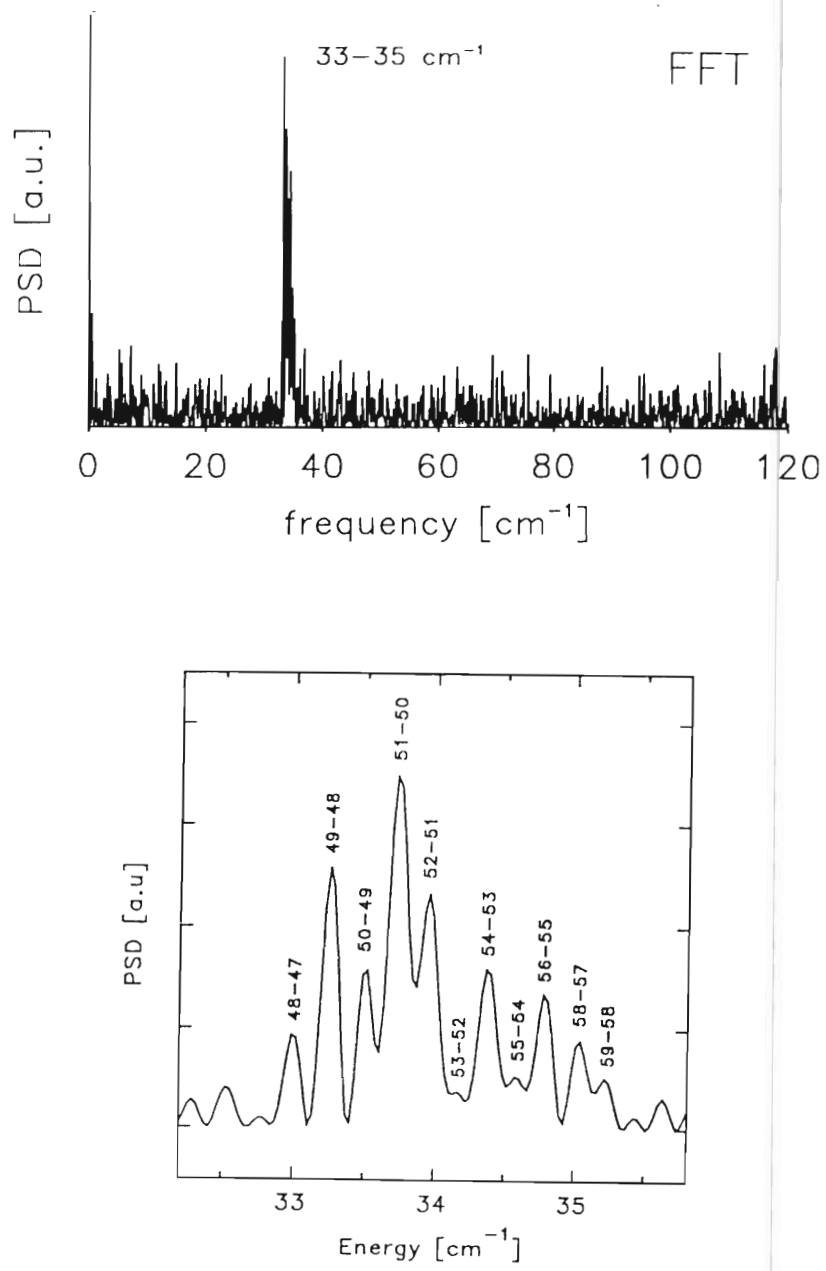

FIG. 7. (upper) Fourier transformation of a 170-ps Na^+ transient measured under the same experimental conditions as the transient displayed in Fig. 6. Only frequencies in the range $33-35\,cm^{-1}$ contribute to the formation of the wavepacket. (lower) Enlargement of the Fourier transformation displayed in the upper figure. The frequency distribution is composed of individual frequencies corresponding to the energy spacings of the vibrational levels forming the wavepacket.

resolved. However, the FFT of a 170-ps-long Na^+ transient, which is not shown, shows frequencies in the range of $33-35\,cm^{-1}$ in the upper part of Fig. 7. In the enlarged lower part of that figure the individual vibrational frequencies are clearly seen. These frequencies are indeed the vibrational energy spacings the wavepacket is composed of, as is proven by the comparison (Table I) with the high-resolution frequency spectroscopy reported by Cooper *et al.* (1984) and Vergès *et al.* (1984). The nanosecond

TABLE I
VIBRATIONAL ENERGY SPACINGS $\Delta G(v)$ IN THE $2\,^1\Sigma_u^+$ STATE FROM FEMTOSECOND DATA

v'	REMPI[a] (cm^{-1})	REMPI[b] (cm^{-1})	FTS[c] (cm^{-1})	Femtosecond experiment (cm^{-1})
59–58	—	—	35.19	
58–57	—	—	35.06	35.1
57–56	35.1	35.5	34.91	
56–55	34.1	34.0	34.75	34.78
55–54	34.5	35.4	34.58	34.65(s)
54–53	34.8	34.4	34.39	34.39
53–52	33.8	33.5	34.20	34.16(s)
52–51	34.5	34.7	33.99	33.98
51–50	35.9	35.4	33.76	33.73
50–49	31.5	33.4	33.53	33.51
49–48	33.3	31.6	33.28	33.27
48–47	33.4	33.7	33.00	33.00
47–46	32.5	33.0	32.71	—
46–45	32.5	33.1	32.40	—
⋮	⋮	⋮	⋮	⋮

Note. Vibrational energy spacings $\Delta G(v)$ obtained from the FFT spectrum displayed in Fig. 7. The letter "s" denotes values obtained from shoulders in Fig. 7. The assignment to v' levels in the $2\,^1\Sigma_u^+$ state is based upon high-resolution Fourier transform spectroscopy (FTS) data. Results of nanosecond laser REMPI experiments are also given.
[a]Delacrétaz and Wöste (1985).
[b]Haugstätter *et al.* (1988).
[c]Cooper *et al.* (1984).

laser REMPI results of Delacrétaz and Wöste (1985) and of Haugstätter *et al.* (1988) are also shown for comparison.

The future experimental work will concentrate on studies of the influence of the barrier on the vibrational wavepacket dynamics. The excitation and detection of a vibrational wavepacket in the $4\,^1\Sigma_g^+$ shelf state of the Na_2 is another example for performing frequency spectroscopy of high lying electronic states in the time domain (Baumert and Gerber, 1994). Note that from transient spectra of the three-dimensional wavepacket motion in Na_3, the normal modes of the excited B-state and of the X-ground state as well have been obtained by an FFT (Baumert *et al.*, 1993b).

B. DYNAMICS OF MULTIPHOTON IONIZATION OF Na_2

In this section we will first give a short introduction to the topic of MPI of small molecules before we present and discuss our results on femtosecond pump–probe experiments on the dynamics of MPI and subsequent fragmentation. Again we have chosen the sodium dimer molecule as a prototype.

Multiphoton ionization of small molecules has been studied by a variety of techniques and is generally well understood. The ionization is predominantly due to REMPI processes, whereas nonresonant multiphoton processes play only a minor role. Dynamical aspects of the interaction of laser radiation with molecules and details of the excitation processes and the different decay channels of highly excited states, embedded in the ionization and in the fragmentation continuum, have rarely been studied up to now. We reported on the interaction of a doubly bound excited molecular state with different continua and the competition between the various decay channels (Baumert *et al.*, 1990). In that study we used femtosecond laser pulses as an experimental tool to distinguish between the dissociative ionization of the molecule and the neutral fragmentation with subsequent excited-fragment photoionization. Both processes are difficult to distinguish when using nanosecond or even picosecond laser pulses. This distinction is of particular importance in multiphoton ionization studies of metal cluster systems (Baumert *et al.*, 1992b). The multiphoton ionization and fragmentation of alkali–metal molecules and, in particular, of Na_2 and Na_3 have attracted considerable current interest. In many experiments with Na_2 it has been found that, in conjunction with the formation of Na_2^+ ions, ionic fragments Na^+ are also formed. REMPI processes via the $A\,^1\Sigma_u^+$ or the $B\,^1\Pi_u$ states are responsible for this observation (Keller and Weiner, 1984; Burkhardt *et al.*, 1985).

Dynamical aspects of the interaction of laser radiation with molecules and details of the excitation and ionization processes can be studied directly in the time domain by femtosecond pump–probe techniques. This allows a closer look at the time scales of the absorption of several photons in molecular multiphoton ionization and the photofragmentation of neutral and ionic molecules, as will be demonstrated in the following parts of this section.

We have reported femtosecond time-resolved multiphoton ionization and fragmentation dynamics of the Na_2 molecule (Baumert *et al.*, 1991a, b). In these experiments we applied photons of 2 eV (around 620 nm) to ionize the Na_2 molecule. At that wavelength it is the $X\,^1\Sigma_g^+$ (Kusch and Hessel, 1978), the $A\,^1\Sigma_u^+$ (Gerber and Möller, 1985), and the $2\,^1\Pi_g$ (Taylor *et al.*, 1983) states that participate in MPI of the neutral molecule. Three photons are needed to ionize the molecule into its ionic ground state, $^2\Sigma_g^+$ (Bordas *et al.*, 1989) (see Fig. 9).

From the real-time observation of vibrational wavepacket motions it was concluded that two different physical processes determine the time evolution of multiphoton ionization. The observed femtosecond pump–probe delay spectrum of the molecular ion (Na_2^+) signal is shown in the upper part of Fig. 8. Evident from the beat structure seen in this transient, there are two frequencies involved and therefore there are two contributions to the transient ionization spectrum. The envelope intensity variation reveals them

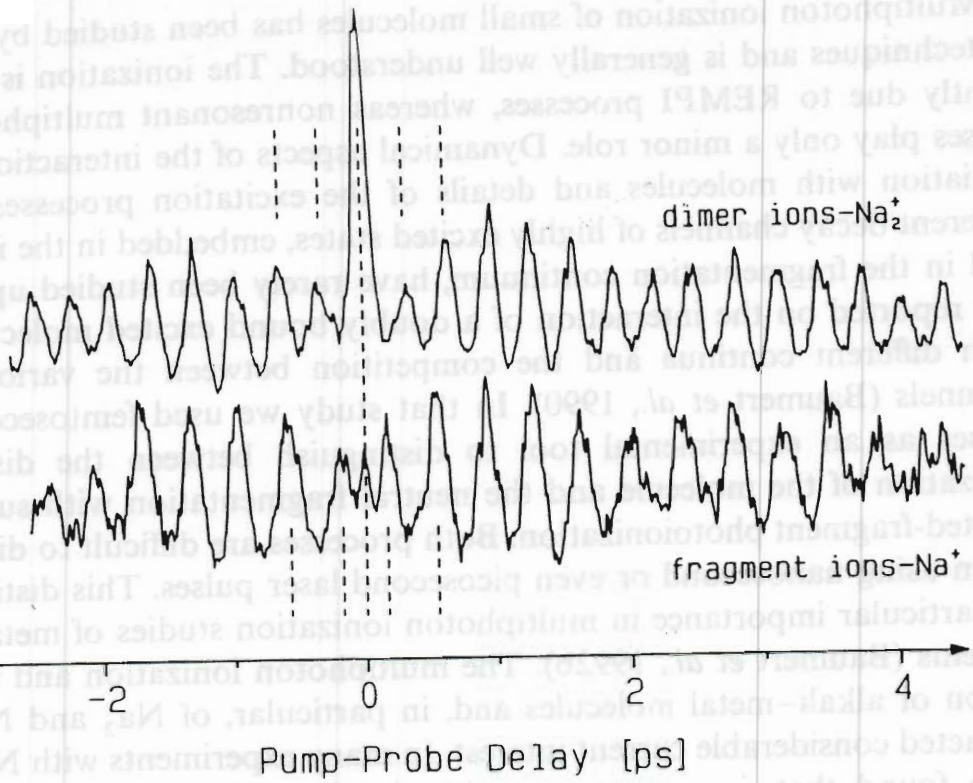

FIG. 8. (upper) Transient Na_2^+ signal obtained as a function of pump–probe delay time between two identical femtosecond laser pulses with 85 fs at $\lambda_{max} = 623$ nm. The envelope intensity variation and the oscillatory structure of this transient Na_2^+ MPI signal reveal two contributions out of phase by 180°. They correspond to independent wavepacket motions in bound molecular potentials with 309 fs ($A\,^1\Sigma_u^+$) and 362 fs ($2\,^1\Pi_g$) oscillation periods. (lower) Transient Na^+ photo fragment signal, obtained under the same experimental conditions as the Na_2^+ transient. The transient shows the dynamics of the 180° phase-shifted $2\,^1\Pi_g$-state wavepacket motion.

to be 180° out of phase. A Fourier analysis of this spectrum yields two groups of frequencies, one centered at 108.1 cm^{-1} and a second one centered at 92.2 cm^{-1}, with an experimental uncertainty of less than 0.5 cm^{-1}. From the observed two oscillation periods, the 180° phase shift and the additionally measured time-resolved Na^+ photofragmentation spectrum (see the lower part of Fig. 8), we concluded that for Na_2 two different MPI processes exist, to require incoherent addition of the intensities to account for the observations.

The direct photoionization of an excited state electron, in which one pump photon creates a vibrational wavepacket in the $A\,^1\Sigma_u^+$ state and two probe photons transfer that motion via the $2\,^1\Pi_g$ state in the ionization continuum, is one (REMPI) process. In this *one-electron* direct photoionization process all three photons are absorbed at the inner turning point. This is therefore an MPI process in which all photons can be absorbed at once or at least within the time duration of the light pulses. The question that has to be addressed now is, why is it that all excitation steps of this MPI process

mainly occur at the inner turning point? This can be discussed by classical arguments, with the help of Mulliken's difference potential concept (Baumert *et al.*, 1991a) and by a quantum mechanical treatment as well (Engel *et al.*, 1993). The results of these two approaches are the same. It is in fact the resonance enhancing $2\,^1\Pi_g$ Rydberg state that restricts the two-photon probe transitions to locations near the inner turning point.

The second MPI process involves excitation of *two electrons* and subsequent electronic autoionization. Here two pump photons create a wavepacket at the inner turning point, in the $2\,^1\Pi_g$ Rydberg state, which then propagates to the outer turning point, where the probe laser transfers the motion into the continuum by exciting a second electron, forming a doubly excited bound neutral Na_2^{**} $(nl, n'l')$ molecule. In this case the probe photon is absorbed at the earliest about 180 fs after the pump photons were absorbed.

In Fig. 9 the relevant potential energy curves taking part in these two different MPI processes are displayed. The two-photon-pump and one-photon-probe ionization process which involves excitation and decay of doubly excited states is indicated. The decay of these doubly excited states takes place by electronic autoionization into the $^2\Sigma_g^+$ ground state of Na_2^+, being responsible for the observed 180° phase-shifted $2\,^1\Pi_g$ wavepacket motion in the Na_2^+ transient (upper part of Fig. 8) and by electronic-autoionization-induced fragmentation, leading to slow Na^+ atomic fragments. This interpretation is confirmed by the observed 180° phase-shifted $2\,^1\Pi_g$ state wavepacket dynamics seen in the Na^+ ionic fragment transient displayed in the lower part of Fig. 8.

Preliminary calculations of doubly excited neutral electronic states of Na_2 correlating with the $Na(4s) + Na(3p)$ asymptote performed by Meyer (1992) show a $^1\Pi_u$ state that can be excited from the outer turning point of the $2\,^1\Pi_g$ state by absorption of one probe photon as indicated in Fig. 10. Although this state can decay by electronic autoionization, it cannot decay by electronic-autoionization-induced fragmentation. This is why there has to be a spin–orbit interaction with the nearby $^3\Pi_u$ doubly excited state via which the fragmentation proceeds.

To give a full account of the problem, the direct photoionization out of the $2\,^1\Pi_g$ state has to be included in the discussions. Again classical methods (Baumert *et al.*, 1991a) as well as quantum mechanical calculations (Engel *et al.*, 1993) can be applied. Note that further excitation of the coherently excited v^* levels of the $2\,^1\Pi_g$ state by a photon of 2 eV leads to a total excitation energy above the dissociation limit of the Na_2^+ $(^2\Sigma_g^+)$ state, and therefore all possible electron kinetic energies according to Franck–Condon considerations can be produced. Analyzing this situation with Mulliken's difference potential concept leads to the result displayed on the left-hand side of Fig. 11. The table of Franck–Condon factors calculated for this probe transition shows four diagonals with high transition probabilities,

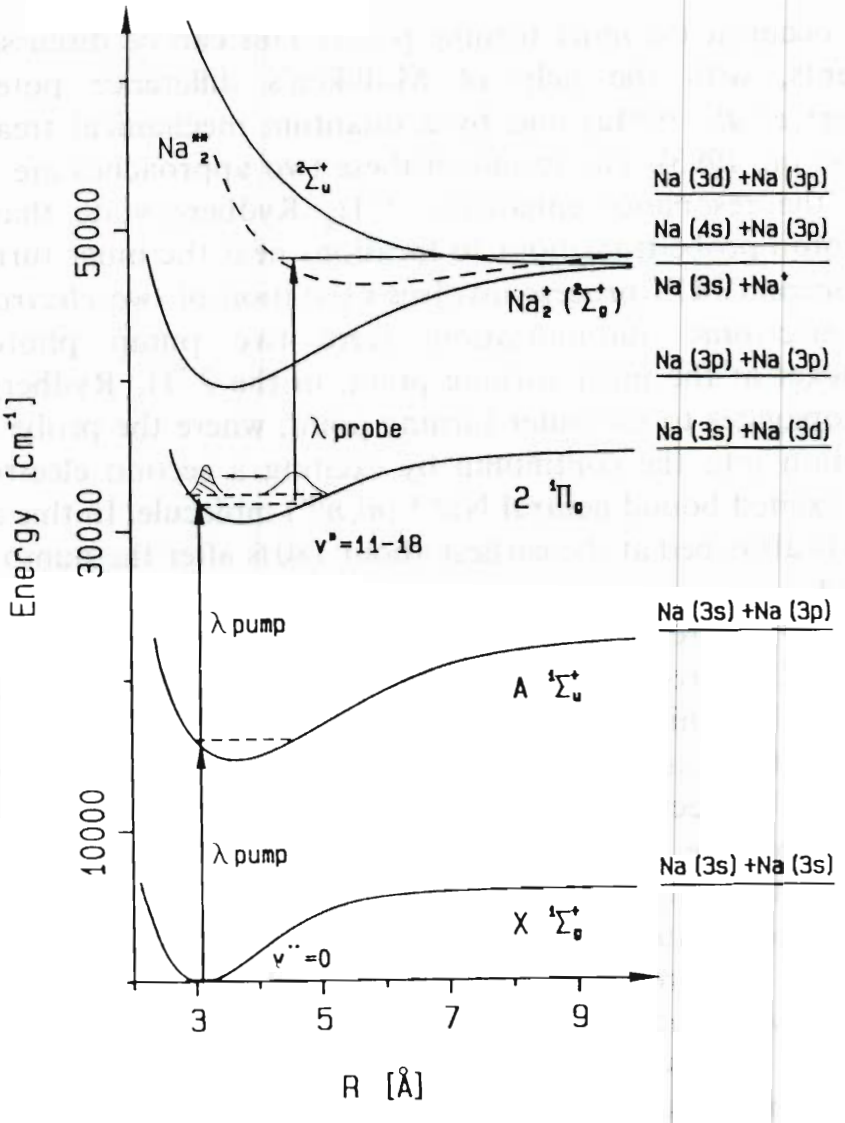

FIG. 9. The relevant potential energy curves of Na_2 taking part in the two different MPI processes are displayed. The two-photon-pump and one-photon-probe ionization processes which involves excitation and decay of doubly excited states is indicated. The dashed line is an estimate for the potential curve of $Na_2^{**}(nl, n'l')$. Calculations of doubly excited states are shown in Fig. 10.

leading essentially to four different electron energies for the considered v^*-vibrational levels. The difference potential $Na_2^+(^2\Sigma_g^+) - Na_2(2\,^1\Pi_g)$ for these four groups of electrons, displayed on the left-hand side of Fig. 11, shows that for each group a different range of internuclear distances is involved in the ionizing transition. However, the different ranges of internuclear distances overlap, and the summation leads to an R-independent transition probability, leading to a time-independent Na_2^+ signal for direct ionization of the oscillating $2\,^1\Pi_g$ wavepacket. In a quantum mechanical calculation by Engel (1991b) this direct ionization process is simulated by "tuning" the probe laser in discrete steps up to the energy of the experiment. For low (ionizing) photon energies a pronounced oscillation, with a period of the oscillating $2\,^1\Pi_g$ wavepacket, is seen on the right-hand side of Fig. 11,

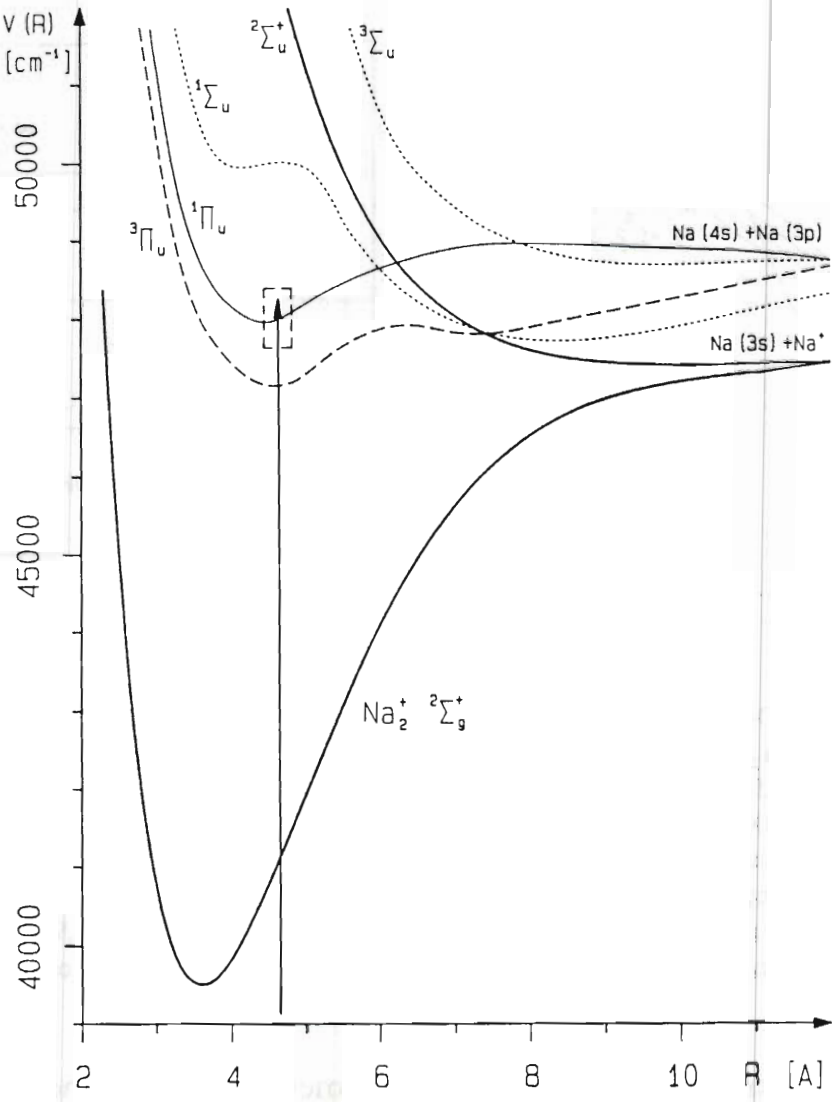

FIG. 10. The potential energy curves of the $^2\Sigma_g^+$ and $^2\Sigma_u^+$ states of Na_2^+ and four doubly excited neutral states of Na_2 are shown. These curves are shown on the basis of unpublished calculations by Meyer (1992). The excitation of the $^1\Pi_u$ doubly excited state by absorption of one probe photon at the outer turning point of the $2\,^1\Pi_g$ state is indicated.

because only low v^+ levels in the Na_2^+ ($^2\Sigma_g^+$) state are accessed. Populating all possible final v^+ states at the experimental laser wavelength, however, leads to a time-independent total Na_2^+ signal.

We performed these experiments with central laser wavelengths of 618 to 627 nm and pulse durations from 70 to 110 fs. For low excitation intensities no change in the global behavior of the measured transients was observed. Only the oscillation periods of the $A\,^1\Sigma_u^+$-state wavepacket and of the $2\,^1\Pi_g$-state wavepacket show slight variations according to the different spectral regions excited.

The Na_2 case is the first example of a femtosecond molecular multiphoton ionization study. It was only through time domain measurements that the existence of a second major ionization process was established. A compre-

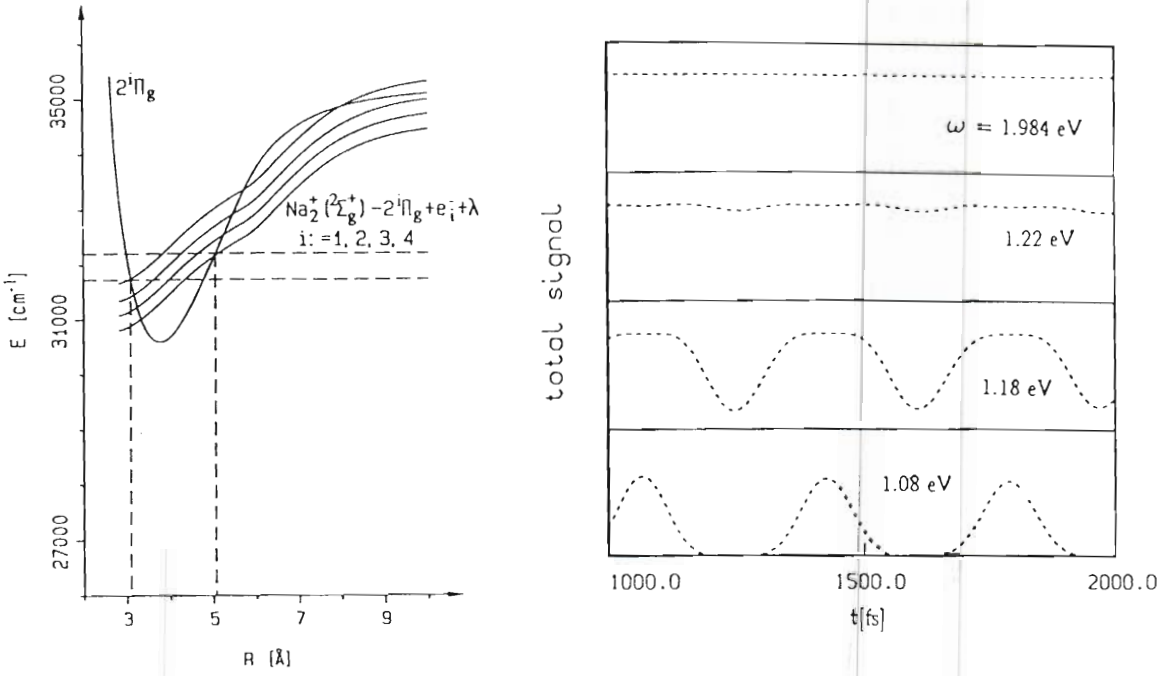

FIG. 11. (left) Difference potential analysis for a direct photoionization process out of the $2\,^1\Pi_g$ state of Na_2. In this bound-continuum transition essentially four different groups of electrons are produced for the coherently excited v^* levels. The electron energies are in the range of 6300–7200 cm^{-1} for laser excitation with 2 eV of photon energy. Although the range of internuclear distances is different for each group, the summation over all electron energies leads to an R-independent ionization signal. (right) Calculated total Na_2^+ signal as a function of pump–probe delay for different laser wavelengths (Engel, 1991b). At 1.984 eV (625 nm) the time dependence for a direct photoionization process out of the $2\,^1\Pi_g$ state of Na_2 has vanished.

hensive discussion based on classical arguments can be found in Baumert *et al.* (1991a), whereas the comparison between experiment and quantum mechanical calculations can be found in Engel *et al.* (1993).

C. Control of Na_2^+ versus Na^+ Yield

In this section we will discuss the Na_2 MPI results from a different point of view. We show that by femtosecond pump–probe techniques basic ideas from the area of control of chemical reactions can be realized.

Controlling a chemical reaction such that a given product is produced at the expense of another, energetically allowed, product is one of the basic issues in physical chemistry. Many publications are devoted to this topic. Some references can be found in a review by Warren *et al.* (1993). As in larger molecules the locally deposited energy redistributes very rapidly—typically on picosecond time scales—throughout the molecule; specially designed pulse shapes and phase-shifted pulses are currently being considered in order to achieve bond selectivity in these systems. For smaller molecular systems, however, the basic ideas of the Tannor–Kosloff–Rice

scheme (Tannor *et al.*, 1986) are applicable. These authors have proposed that controlling the duration of propagation of a wavepacket on an excited electronic potential energy surface, by simply controlling the time delay between pump and probe pulses, can be used to generate different chemical products. This idea was realized in an experiment by Zewail and co-workers (Potter *et al.*, 1992a). They used two sequential coherent laser pulses to control the reaction of I_2 molecules with Xe atoms to form XeI. It was shown that the yield of product XeI is modulated as the delay between the pulses is varied, reflecting its dependence on the nuclear motions of the reactants. However, an example of how the propagation of wavepackets can be used to produce one product at the expense of another energetically allowed product is given by our experiments for the first time, according to our knowledge.

In order to better illustrate the topic, let us assume that we focus a nanosecond laser, having a photon energy of about 2 eV, on our molecular beam. After absorption of three photons we will detect Na_2^+ and Na^+ in our TOF spectrometers according to the two ionization processes described before. There are no simple means of producing Na_2^+ at the expense of Na^+ with this nanosecond laser at a fixed intensity and wavelength. Using the time-resolved approach, we know that at the inner turning point of the

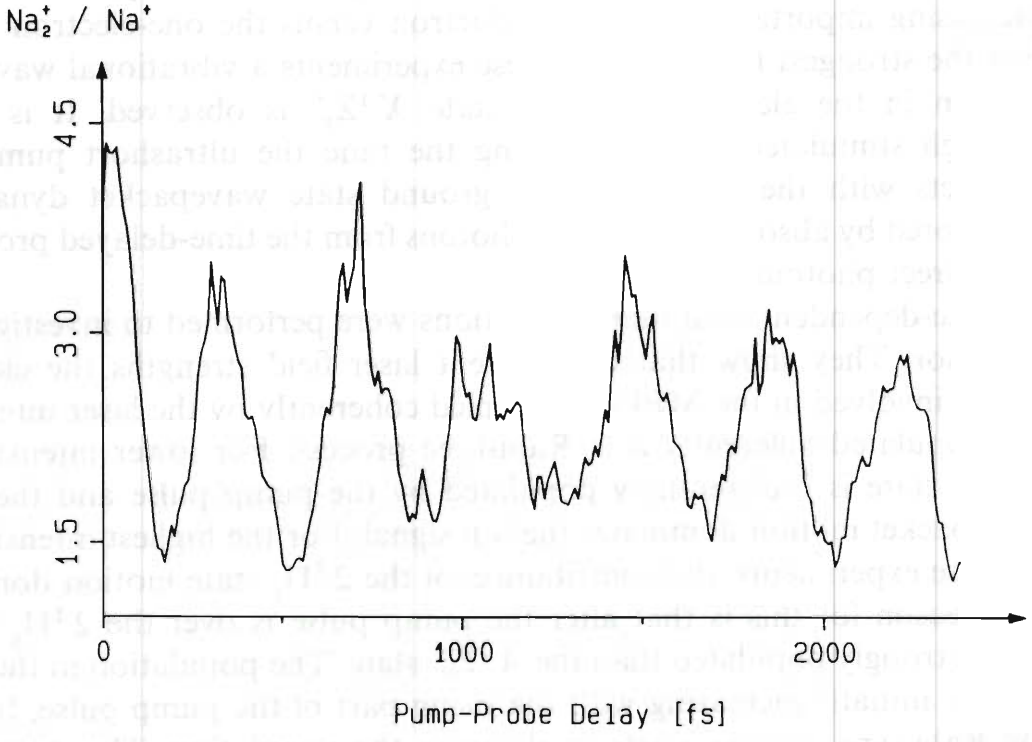

FIG. 12. Controlling a chemical reaction such that a given product is produced at the expense of another, energetically allowed, product is of general interest in physics and chemistry. Here we apply femtosecond pump–probe techniques in order to control the internuclear distance of the molecule Na_2. According to the different MPI processes this leads to a strongly varying Na_2^+/Na^+ ratio with respect to the pump–probe delay time.

$A\,^1\Sigma_u^+$ and $2\,^1\Pi_g$ states in Na_2 the molecule is directly ionized by the probe laser, whereas only at the outer turning point of the $2\,^1\Pi_g$ state fragment ions of Na^+ are produced by exciting the neutral doubly excited state with its subsequent decay channels (Fig. 9). Thus by controlling the duration of propagation of the wavepackets on the $A\,^1\Sigma_u^+$ and $2\,^1\Pi_g$ states in Na_2 we are able to produce Na_2^+ at the expense of Na^+ by adjusting the pump–probe delay time. This is illustrated in Fig. 12, in which we display the ratio of the Na_2^+ signal over the Na^+ signal from Fig. 8. A modulation of this ratio by at least a factor of 2 is seen as a function of pump–probe delay.

D. High Laser Field Effects in Multiphoton Ionization of Na_2

In a further study the dependence of the total Na_2^+ ion signal on the intensity of the femtosecond pulses was investigated in detail (Baumert *et al.*, 1992c). The experimental results, shown in the upper part of Fig. 13, were obtained for three different intensities ($I_0 = 10^{12}$ W/cm^2, $0.3*I_0$, and $0.1*I_0$). The curves exhibit periodic oscillations with different periods for different laser intensities. The periodic contributions to these transients were analyzed by taking their Fourier transform, displayed in the lower part of Fig. 13. Additionally for higher laser intensities the relative contributions from the $A\,^1\Sigma_u^+$ and the $2\,^1\Pi_g$ states change dramatically, indicating the increasing importance of the two-electron versus the one-electron process. For the strongest fields used in these experiments a vibrational wavepacket motion in the electronic ground state $X\,^1\Sigma_g^+$ is observed. It is created through stimulated emission during the time the ultrashort pump pulse interacts with the molecule. This ground state wavepacket dynamics is monitored by absorption of three photons from the time-delayed probe laser in a direct photoionization process.

Time-dependent quantum calculations were performed to investigate this behavior. They show that for different laser field strengths the electronic states, involved in the MPI and coupled coherently by the laser interaction, are populated differently in a Rabi-type process. For lower intensities the $A\,^1\Sigma_u^+$ state is preferentially populated by the pump pulse and the $A\,^1\Sigma_u^+$ wavepacket motion dominates the ion signal. For the highest intensity used in these experiments, the contribution of the $2\,^1\Pi_g$ state motion dominates. The reason for this is that after the pump pulse is over the $2\,^1\Pi_g$ state is more strongly populated than the $A\,^1\Sigma_u^+$ state. The population in the $A\,^1\Sigma_u^+$ state is initially increasing with the rising part of the pump pulse, but then the Rabi-type process starts to decrease the population. This behavior is nicely illustrated in Fig. 14 for four different laser intensities [for computational details, see Baumert *et al.* (1992c) and Meier (1992)]. Thus by changing the intensity of the femtosecond pump laser one may selectively control the relative strength of the direct one-electron photoionization versus the two-electron excitation and electronic autoionization process.

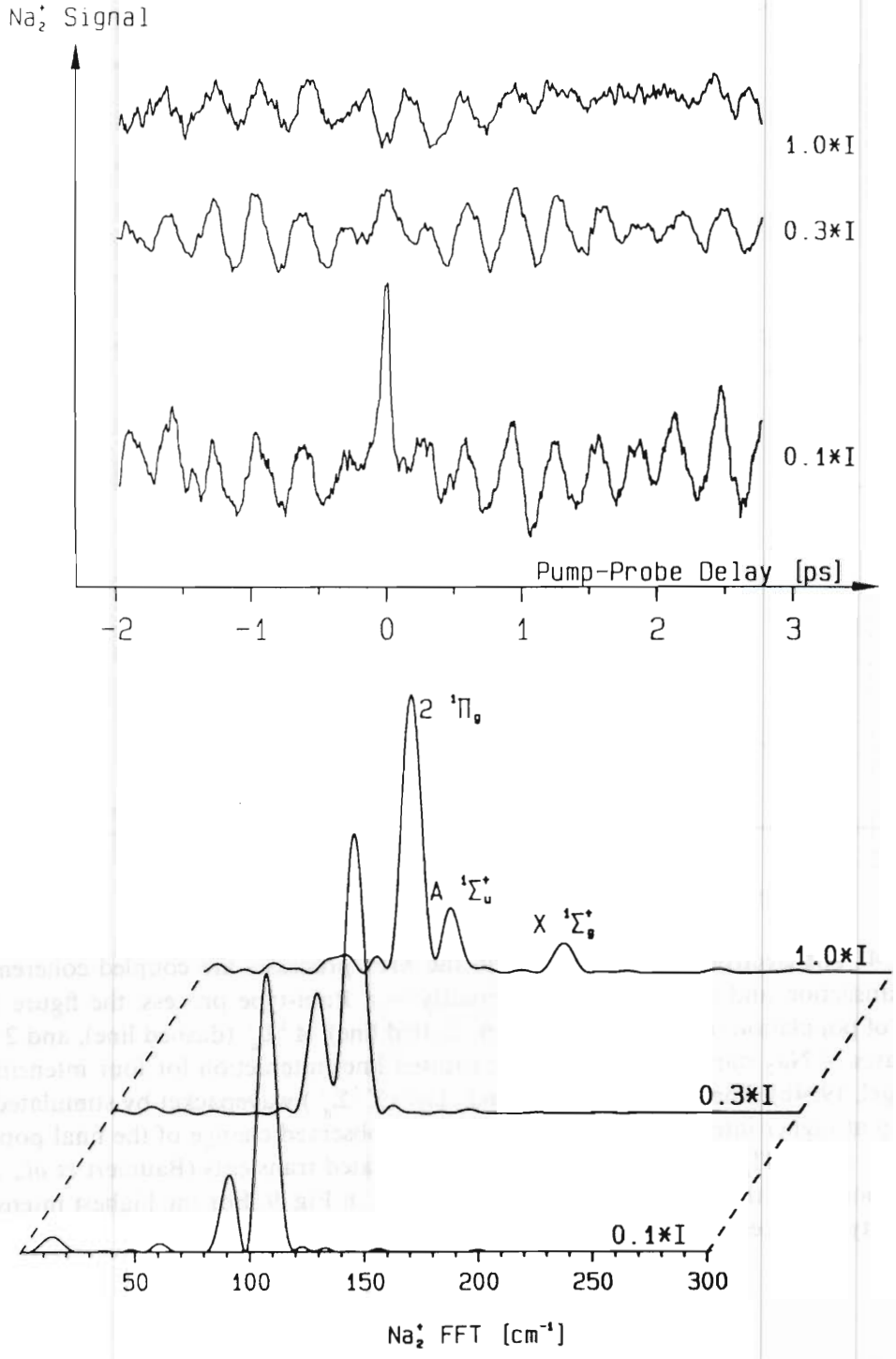

FIG. 13. The upper figure shows transient Na_2^+ spectra as a function of delay time between pump and probe pulses. Different intensities were used as indicated. In the lower figure, the Fourier transforms of the transient spectra are displayed. Note the dramatic change of the Fourier amplitudes as a function of intensity. At $1.0 \cdot I$ a contribution of the $X\ ^1\Sigma_g^+$ ground state wavepacket to the transient ionization spectrum is observed in the Fourier spectrum.

This intensity-dependent effect could be used in addition to the delay time variation to optimize the control scheme discussed in the previous section. The coherent coupling of the electronic states as a function of laser intensity is expected to influence the total ionization yield as well as the kinetic energy of the ejected photoelectrons (Meier and Engel, 1994c).

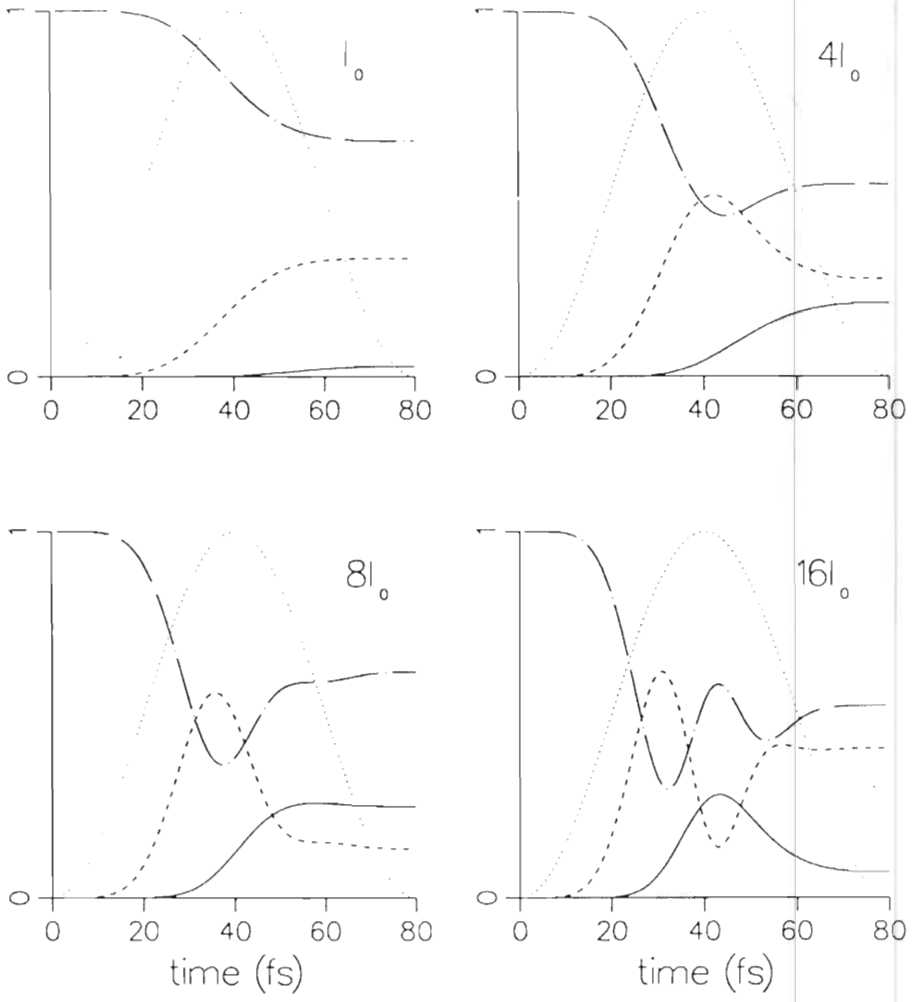

FIG. 14. The electronic states involved in the MPI processes are coupled coherently by the laser transaction and also populated differently in a Rabi-type process: the figure shows the change of population in the $X\,^1\Sigma_g^+$ (dashed–dotted line), $A\,^1\Sigma_u^+$ (dashed line), and $2\,^1\Pi_g$ (solid line) states of Na_2 during the pump pulse (dotted line) interaction for four intensities (Meier and Engel, 1994b). The creation of a ground-state ($X\,^1\Sigma_g^+$) wavepacket by stimulated emission pumping at higher intensities is seen as well as the observed change of the final population of the $A\,^1\Sigma_u^+$ and $2\,^1\Pi_g$ states (I_0, $4I_0$, and $8I_0$). Calculated transients (Baumert *et al.*, 1992c) are in agreement with the measured transients displayed in Fig. 9. For the highest intensity ($16I_0$) the Rabi-type process is clearly seen.

IV. Results and Discussion of Experiments in Cluster Physics

A. Dynamics of Na_n^+ Photofragmentation

The stability and fragmentation dynamics of metal cluster ions formed through laser photoionization are a major issue in cluster physics. In particular for sodium and potassium cluster ions, Bréchignac *et al.* (1987) have reported that the predominant fragmentation channels, the evaporation of neutral monomers and dimers, respectively, are associated with microsecond fragmentation times due to sequential evaporation of mono-

mers and dimers caused by cluster heating. To improve the understanding of the stability and fragmentation of metal clusters and the dynamics during and immediately after the photoionization event and to determine the size of the ejected particles, experiments with femtosecond time resolution are performed (Baumert *et al.*, 1992b). Ultrashort light pulses of 60 fs duration are used to photoionize the neutral sodium cluster in the beam and to induce the fragmentation. The time-delayed identical probe laser pulses photoionize the neutral photofragments, ejected by the cluster ions. Time-of-flight spectroscopy is used to determine the mass of the ion and the initial kinetic energy of the probe-laser-ionized fragments. Note that for laser pulse durations of 60 fs, which are considerably shorter than the cluster vibrational periods of a few hundred femtoseconds, the clusters are nearly frozen during the photoionization event. So it is questionable whether cluster heating in femtosecond photoionization plays any role and whether sequential evaporative cooling occurs.

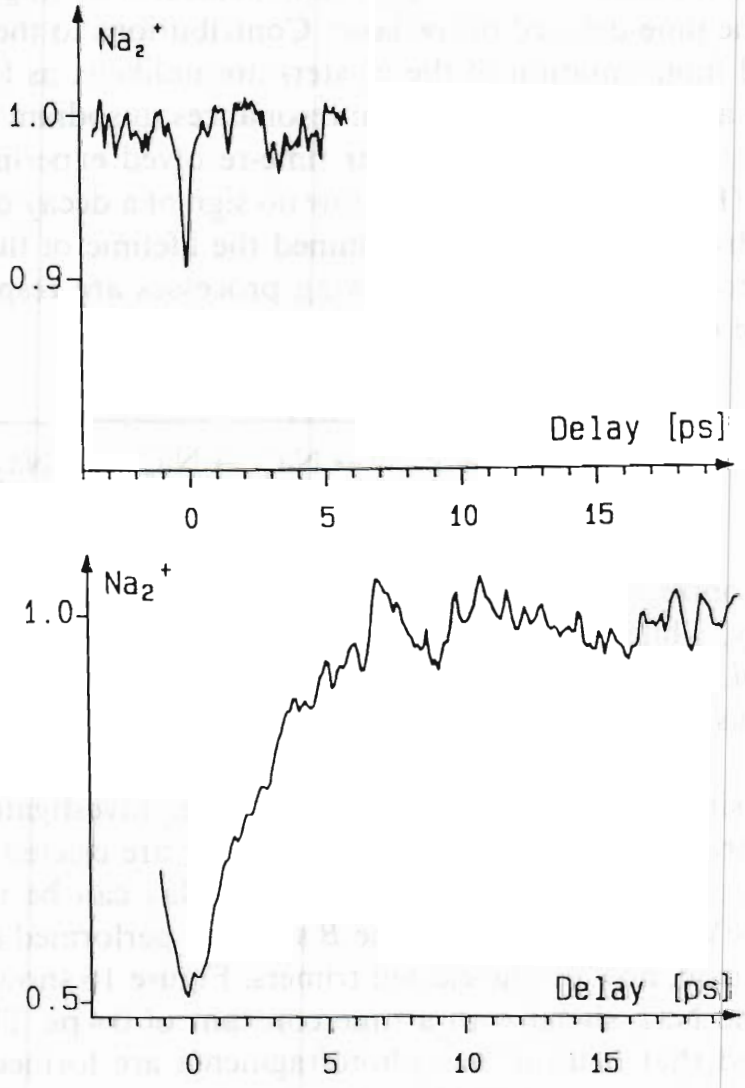

FIG. 15. Transient Na_2^+ signal in a molecular beam (top) and in a cluster beam (bottom). The ejection of Na_2 is due to ionic Na_n^+ cluster fragmentation. The rise time of the Na_2^+ signal is 2.5 ps.

The lower part of Fig. 15 shows the observed transient Na_2 fragmentation spectrum. The signal is symmetric around zero time delay, because we use identical pump and probe laser pulses. The buildup of the Na_2^+ probe signal strongly depends on the pump–probe delay time and shows a rise time of 2.5 ps. This transient was measured with a seed gas pressure of 8 bar for the cluster beam. In order to prove that this rise time is due to ionic cluster fragmentation we reduced the seed gas pressure to 0.1 bar. At that pressure there are virtually no clusters with $n > 3$ in the beam. The corresponding transient Na_2^+ spectrum, displayed in the upper part of Fig. 15, shows only a small narrow dip at time zero. This is due to the fragmentation of Na_2^+ by the enhanced laser intensity from the temporal overlap of pump and probe pulses.

The increase of the Na_2^+ probe signal is due to the fragmentation processes of Na_n^+ clusters ($n \geqslant 3$). The neutral sodium clusters are ionized by the pump laser, followed by a fragmentation into Na_2 and other channels, as will be described below. The neutral Na_2 fragments are then ionized by the time-delayed probe laser. Contributions to the Na_2^+ transient from neutral fragmentation of the clusters are unlikely, as for 2 eV photon energy there are no strong absorption resonances in sodium clusters, except for the B state of Na_3. However, our time-resolved experiments on the B state of Na_3 (Baumert *et al.*, 1993b) show no sign of a decay on a picosecond time scale. Broyer *et al.* (1988) determined the lifetime of the B state to be 14 ns. Therefore we believe the following processes are responsible for the observed rise of the Na_2^+ signal.

Pump	$Na_n + k \cdot h\nu \rightarrow Na_n^+ \rightarrow Na_{n-2}^+ + Na_2$
Probe	$Na_2 + j \cdot h\nu \rightarrow Na_2^+$

In order to ionize Na_n ($n = 2, 4, 6, 8$) at $\lambda = 618$ nm at least three photons are necessary, while for all other masses at least two photons are needed (Kappes *et al.*, 1988). Note that for a probe laser ionization with more than three photons a fragmentation of Na_2^+ into $Na^+ + Na$ is energetically possible.

An increasing question which had not been investigated before was whether neutral fragments such as Na_3 and Na_4 are ejected in dissociative photoionization of larger sodium clusters. As Na_3 can be ionized by two photons of 2 eV photon energy via the B state we performed a pump–probe experiment again, now on the ejected trimers. Figure 16 shows the observed buildup of the Na_3^+ signal with a time constant of 0.4 ps. This experiment clearly proved that neutral Na_3 photofragments are formed and that the ejection time scale is extremely fast. As it has been discussed in Baumert *et al.* (1992b), we believe the fragmentation of Na_8^+ into Na_5^+ and Na_3 is mainly responsible for the observed neutral trimer signal.

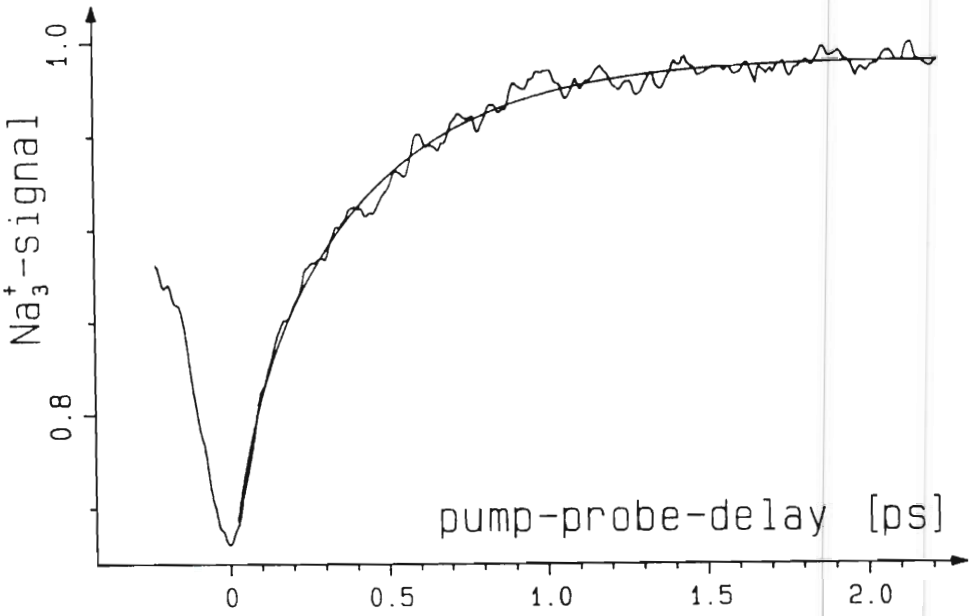

FIG. 16. Pump–probe delay spectrum of the ejected neutral trimer fragments Na_3. The probe signal Na_2^+ buildup time constant of 0.4 ps indicates a direct photoinduced fragmentation of sodium cluster ions rather than a statistical unimolecular decay.

In the discussion of the stability of metal cluster ions against fragmentation, it is often assumed that photoinduced electronic excitation is strongly coupled and relaxed to internal modes. The excess energy from successive absorption of photons in photoionization is thought to be quickly redistributed between the vibrational modes of the cluster ion, leading to statistically dominated fragmentation. However, the observed rise time of 2.5 ps (Na_2^+) and 0.4 ps (Na_3^+) is much too fast for an efficient relaxation of electronic energy in a cluster.

In conclusion, we find that the ejection of dimer Na_2 and trimer Na_3 photofragments occurs on ultrashort time scales of 2.5 and 0.4 ps, respectively. This and the absence of cluster heating reveal that direct photoinduced fragmentation processes are important at short times rather than the statistical unimolecular decay.

B. Dynamics of the Neutral Na_4 Resonance at 680 nm

In this section the cluster Na_4 is taken as an example to demonstrate how we obtain the spectroscopy, the dynamics, and the decay channels of neutral metal clusters by employing femtosecond laser techniques. Figure 17 shows the absorption spectrum of the cluster sizes Na_4 to Na_7, studied by multiphoton ionization with tunable femtosecond laser pulses. The observed spectrum of Na_4 is similar to absorption spectra measured by nanosecond laser depletion spectroscopy (Wang *et al.*, 1990). The Na_4 intermediate

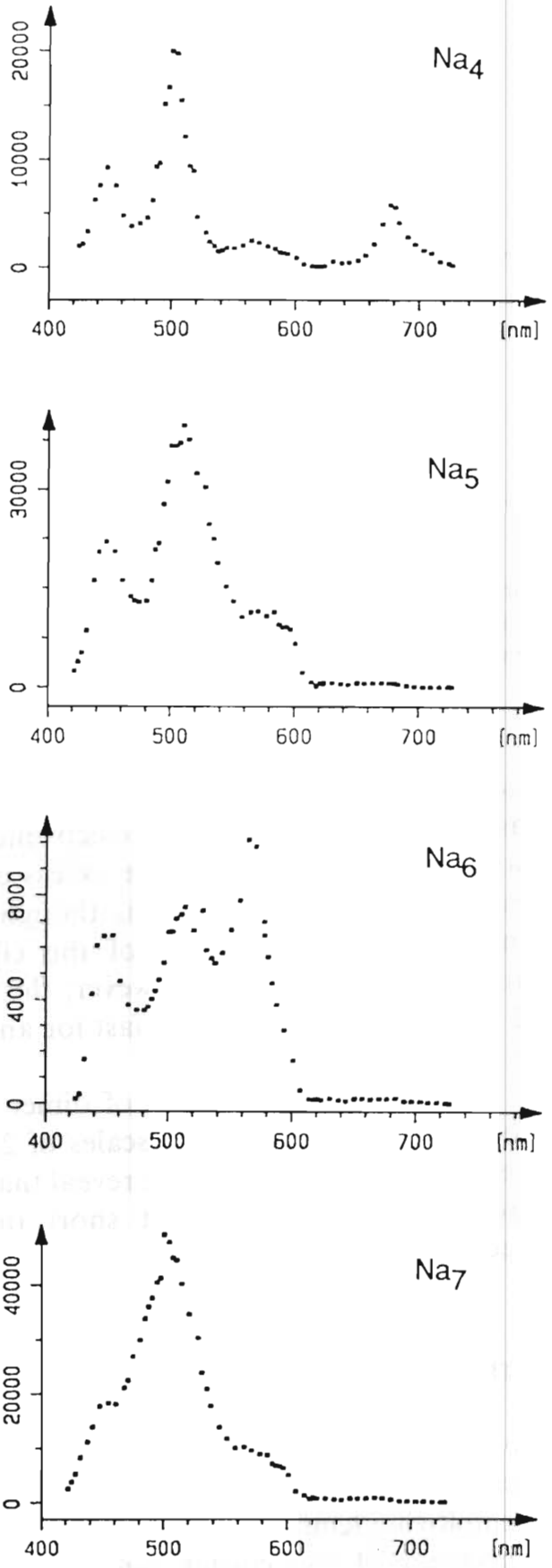

FIG. 17. Absorption spectrum of Na_4 to Na_7 measured by multiphoton ionization with tunable femtosecond laser pulses. Note that only the Na_4 has an absorption band at 680 nm.

resonance at 680 nm is chosen to demonstrate how the femtosecond pump–probe technique is ideally suited to investigate neutral cluster photofragmentation. All larger cluster sizes, Na_n with $5 < n \leqslant 21$, show little photoabsorption strength in this wavelength regime. Therefore contributions from fragmentation of larger cluster masses to the photodissociation signal and to the observed dynamics can be neglected. The actual femtosecond pump–probe experiment to study the decay of the intermediate Na_4^* resonance was carried out at 694 nm and resulted in the transient Na_4^+ signal shown in Fig. 18. Since pump and probe pulses are identical, the spectrum is symmetric with respect to time zero. The decrease of the signal to longer delay times reflects the decay of the intermediate resonance. The decay curve can be represented by a single exponential with a time constant of 0.74 ± 0.05 ps. The question which has to be addressed now is, what is the physical origin of the decay? There are two possibilities (which do not exclude each other): either the energy is redistributed among the other degrees of freedom in the cluster or the decay is attributed to an instantaneous photodissociation. The latter should lead to formation of neutral fragments Na_n ($n < 4$), with a buildup time being comparable to the decay time observed for the Na_4 parent cluster.

The sodium trimer Na_3 is the most studied and best known small metal cluster. Its absorption spectrum was first measured by the Wöste group (Broyer *et al.*, 1986a, b), employing nanosecond two-photon ionization spectroscopy and also depletion spectroscopy and later by the Kappes group (Wang *et al.*, 1990) using depletion spectroscopy.

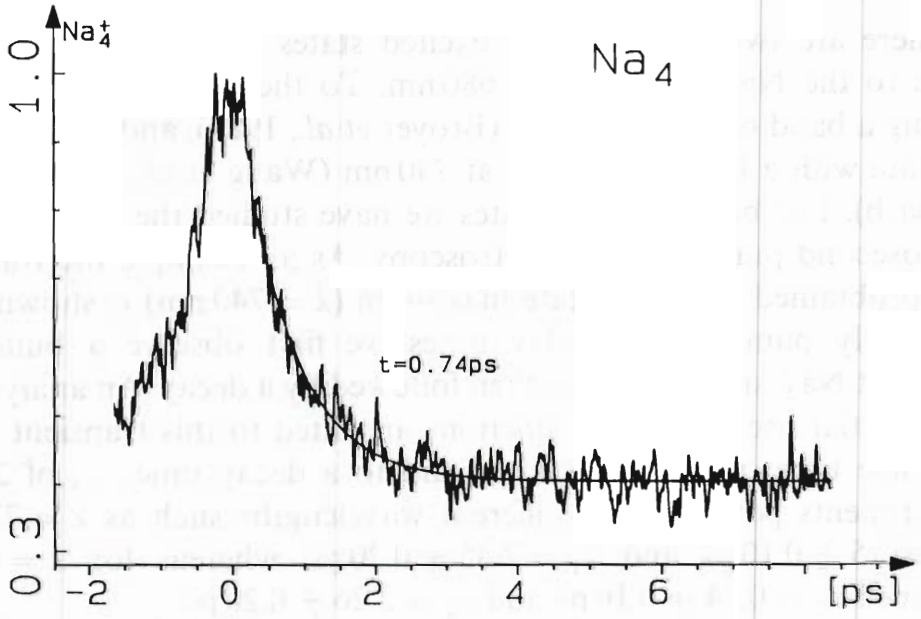

FIG. 18. Decay of the Na_4 absorption resonance (Fig. 17) measured in a pump–probe experiment at 694 nm. The decay time determined by fitting a single exponential is 0.74 ± 0.05 ps.

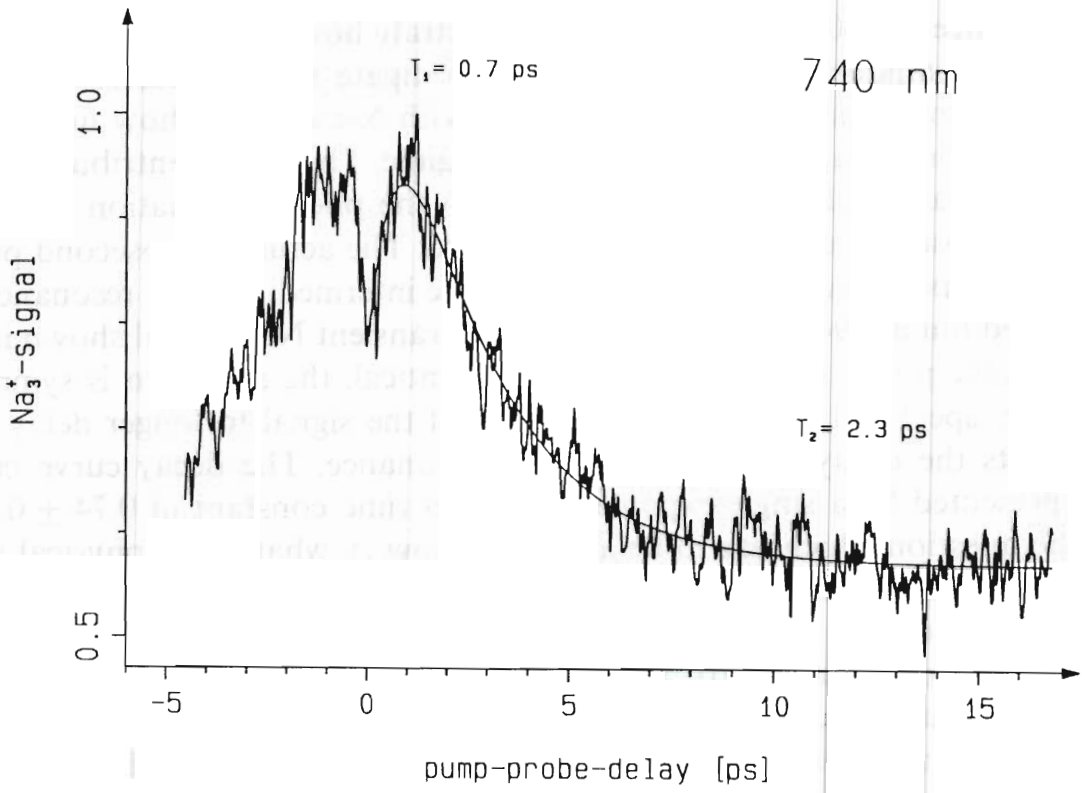

FIG. 19. Transient Na_3 spectrum as a function of pump–probe delay time. The maximum A'-state absorption of Na_3 is at 740 nm. Fitting exponential rise and decay functions to this transient gives a rise time, τ_2, of 0.7 ± 0.1 ps and a decay time, τ_1, of 2.3 ± 0.2 ps. Similar rise times for Na_3 transients were measured at 668 and 731 nm (see the text). The rise time of the Na_3 transients reflects the decay of an Na_4^* resonance (Fig. 18), while the decay time is the lifetime of the Na_3 A' state.

There are two electronically excited states of Na_3, whose energies are close to the Na_4 resonance at 680 nm. To the blue side it is the A state, having a band origin at 675 nm (Broyer *et al.*, 1988), and to the red side, the A' state with a band maximum at 740 nm (Wang *et al.*, 1990; Broyer *et al.*, 1986a, b). For both of these states we have studied the decay dynamics by femtosecond pump–probe spectroscopy. As an example the transient Na_3^+ signal obtained at the A' state maximum ($\lambda = 740$ nm) is shown in Fig. 19. For early pump–probe delay times we first observe a buildup of the transient Na_3^+ signal which is then followed by a decay. An analysis in which exponential rise and decay functions are fitted to this transient curve leads to a rise time, τ_2, of 0.7 ± 0.1 ps and to a decay time, τ_1, of 2.3 ± 0.2 ps. Experiments performed at different wavelengths such as $\lambda = 731$ nm gave $\tau_2 = 0.75 \pm 0.10$ ps and $\tau_1 = 2.35 \pm 0.20$ ps, whereas for $\lambda = 668$ nm we obtained $\tau_2 = 0.74 \pm 0.10$ ps and $\tau_1 = 2.26 \pm 0.20$ ps.

Note that the excitation wavelengths used in these three experiments with Na_3 are close to the 680-nm resonance of Na_4 (Fig. 17). Note also that the derived buildup times, τ_2, of the Na_3^+ transients for the three excitation wavelengths match the decay time of the observed Na_4 transient (Fig. 18).

The conclusion we draw from this is that excitation of Na_4 in this wavelength region leads to an instantaneous fragmentation of the neutral excited Na_4^* into neutral excited Na_3^* and atomic Na.

Now we turn to the question of what geometric structure of Na_4 can be derived from the absorption spectrum measured by femtosecond multiphoton ionization spectroscopy. Configuration interaction (CI) calculations by Bonacic-Koutecky *et al.* (1990a) lead to two different geometric structures for Na_4. One is a planar rhomboidal structure with D_{2h} symmetry; the other is a slightly tilted three-dimensional tetrahedral structure, being 0.256 eV higher in total energy. The femtosecond multiphoton ionization spectrum of Na_4 (top of Fig. 17) as well as depletion spectroscopy results obtained by Wang *et al.* (1992) show resonances at 1.80, 2.20, 2.45, and 2.75 eV. Dipole allowed transitions for the planar geometry were calculated for 1.71, 2.07, 2.45/2.46, and 2.76 eV and are in good agreement with the experimental results. The calculated spectrum of the three-dimensional structure consists mainly of only one transition at 2.12 eV and therefore does not agree with the experiments. Results obtained by applying the ZEKE technique to the study of Na_4 are also consistent with a planar rhomboidal structure (Thalweiser, 1992). The same conclusion had already been reached and reported by Wang *et al.* (1990).

C. Na_n Cluster Resonances and Their Decay Dynamics

One of the topics in metal cluster physics is to pursue the change from molecular to metallic behavior. In that context it is very instructive to investigate the electronic excitations of metal clusters. In a molecular picture the electronic excitations are treated with quantum chemical methods. In the case of sodium clusters, which are convenient for theoretical studies, because there is only one valence electron per atom, full CI calculations were performed on clusters with up to four atoms (Bonacic-Koutecky *et al.*, 1990a). The larger Na_n clusters ($n = 5$–20) were treated by employing *ab initio* effective core potentials (Bonacic-Koutecky *et al.*, 1990b, 1992). In quantum chemical calculations the detailed geometric structure of the cluster is essential. For several sodium cluster sizes Bonacic-Koutecky *et al.* (1990a, 1992) calculated the electronic excitations belonging to energetically low lying geometric structures.

However, in the past another model, the free electron model, has often been used to discuss the electronic excitations of metal clusters. In that treatment the most simple approach is the jellium model, in which the delocalized electrons are assumed to move in a constant, smeared out positively charged background (Eckardt, 1984a). This approach was reviewed by de Heer (1993) and Brack (1993). In the jellium model the detailed positions of the cluster atomic ionic cores play no role. Eckardt and Penzar (1988), Penzar and Eckardt (1990), and Eckardt (1984b) calculated

the electronic structure of Na_n clusters self-consistently within the density functional theory (DFT). The electron correlation was taken into consideration by the local density approximation (LDA) and by time-dependent LDA (TDLDA) (Eckardt and Penzar (1991). Another approach was discussed by Clemenger (1985), who assumed that the cluster electrons are moving in a harmonic oscillator potential and are restricted to spheres and spheroids as the possible cluster geometries. This concept originated from nuclear physics. Selby *et al.* (1989) extended this model to ellipsoidal clusters. Originally Mie (1908) calculated light absorption and diffraction of small metal spheres within classical electrodynamics. Nowadays a modified Mie model is used to explain the absorption spectra of metal clusters (Wang *et al.*, 1990). For the spherical clusters Na_8 and Na_{20} that model predicts a single homogeneously broadened surface plasmon resonance. Applying more elaborate techniques like time-dependent density–functional theory to the study of the photoabsorption spectrum of closed-shell sodium clusters within the spherical jellium model leads to a splitting of the Na_{20} absorption resonance (Rubio *et al.*, 1992). Configuration interaction calculations of jellium clusters by the nuclear shell model (Koskinen *et al.*, 1994) give a single peak result of the Na_{20} resonance. Only when the calculations are restricted to lower excitations is a two-peak absorption spectrum calculated. In the latter publication no splittings were calculated for the Na_8 resonance.

Experimentally the absorption spectra of metal clusters were measured by means of depletion spectroscopy (Selby *et al.*, 1989; Wang et al., 1990). Due to the very short-lived excited states of Na_n clusters with $n > 3$ the well-known method of REMPI spectroscopy with nanosecond laser pulses fails. In depletion spectroscopy the ion signal decrease (due to cluster fragmentation after the interaction with nanosecond laser pulses) is detected as a function of the laser wavelength.

As discussed in Section IV.B we employed REMPI spectroscopy with tunable femtosecond laser pulses to investigate the absorption resonances in the wavelength region of 420 to 750 nm. Additionally femtosecond pump–probe techniques are introduced to investigate the decay dynamics of intermediate resonances.

In the framework of the jellium model, the Na_8 cluster is predicted to be a spherically symmetric metallic particle. During laser pulses about 100 fs in duration the clusters are excited and ionized by the absorption of photons out of the same laser pulse. Due to the very short pulse duration the clusters do not fragment during the interaction time as would be the case with nanosecond laser pulses. Therefore femtosecond REMPI spectroscopy is, besides depletion spectroscopy, a well-suited technique to measure the absorption spectrum of size-selected neutral metal clusters. It is necessary to notice that, besides the excitation step, the ionization of the excited cluster states may influence the spectral intensity distribution of the cluster spectra.

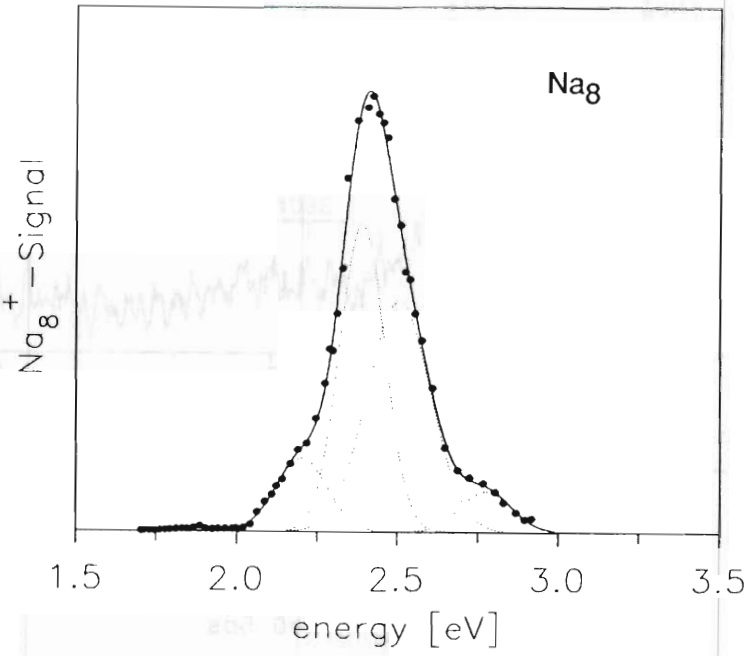

FIG. 20. Absorption spectrum of Na_8 measured by multiphoton ionization with tunable femtosecond laser pulses. Taking Gaussian line shapes into account, four different resonance contributions are derived from the analysis of the measured spectrum.

This may slightly affect the strength of the different spectral components of the cluster resonances. Depletion spectroscopy on the other hand suffers from neutral fragmentation of larger cluster masses, which would affect the observed absorption spectrum of a specific cluster size.

Figure 20 shows the Na_8 femtosecond REMPI spectrum from 1.7 to 2.9 eV. The spectrum is normalized to a constant laser intensity. In addition the absorption spectra for Na_n cluster sizes of $n = 4$ to $n = 21$ were measured. In Fig. 20 the solid line through the data points is based upon a fit of the experimental data with a sum of gaussian functions. The experimental data are best represented by a sum of four gaussian functions. The central energies of the four contributions are 2.2, 2.39, 2.49, and 2.78 eV. Our measurements of the absorption spectra of different cluster sizes agree very well with the corresponding spectral curves obtained by depletion spectroscopy (Selby *et al.*, 1989; Wang *et al.*, 1990). These results from two different experiments clearly disagree with the simple picture of a single homogeneously broadened surface plasmon resonance due to the spherical shape of Na_8. On the other hand the experimentally determined positions of the four Na_8 resonances are in much better agreement with quantum chemical calculations by Bonacic-Koutecky *et al.* (1990b, 1992). In the case of Na_8 the best agreement between calculation and experimentation is achieved assuming a T_d-cluster geometry. This shows that the detailed geometric structure of this cluster is essential in understanding the multiple resonances.

In Fig. 21 three transient ionization spectra of Na_8 are displayed. Each was obtained with the femtosecond laser tuned to the individual resonances

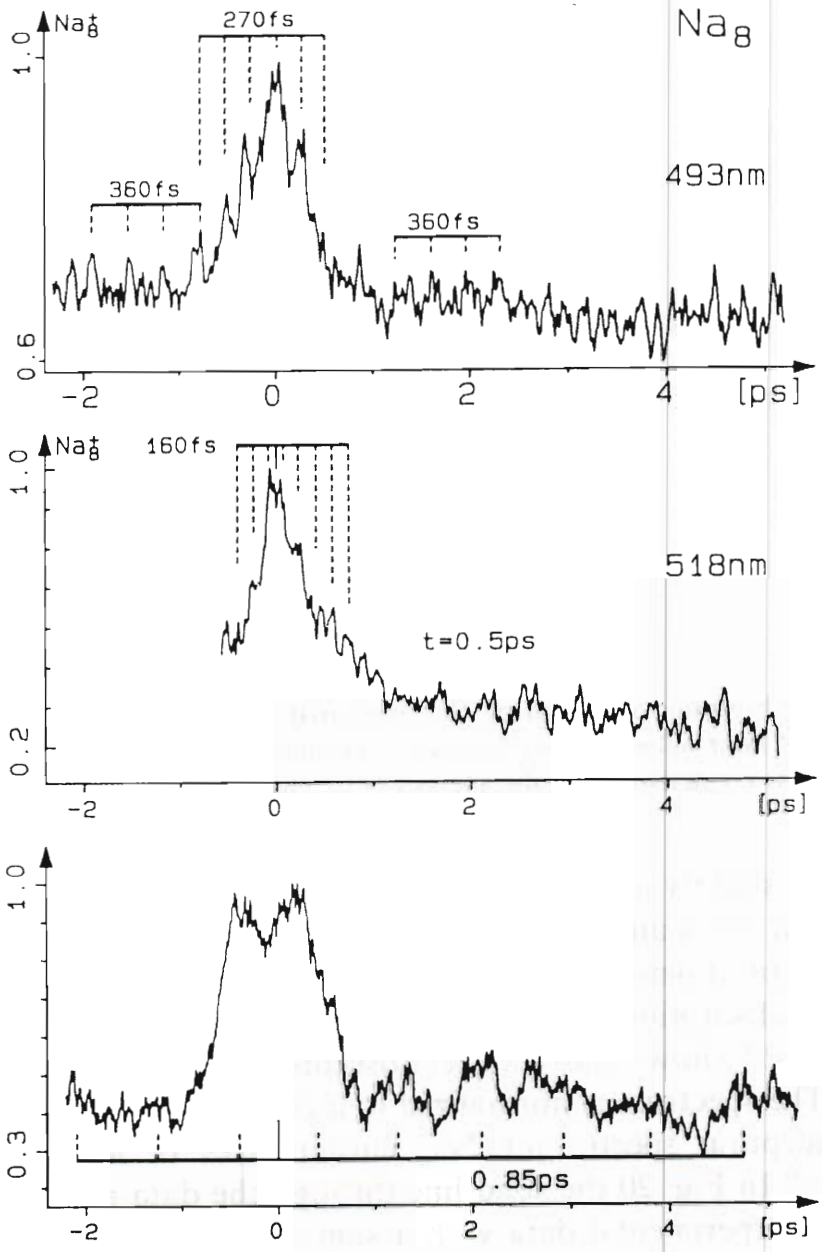

FIG. 21. Femtosecond time-resolved decay of Na_8^* intermediate states. The laser wavelengths are tuned to the individual resonances at 493, 518, and 540 nm as shown in Fig. 20.

in Fig. 20. The pump pulse excites the Na_8 cluster while the time-delayed identical probe pulse probes the coherence and residual population by photoionizing Na_8^*, the intermediate excited electronic states. As already discussed we have applied this technique to Na_2, Na_3, Na_4, and Na_n^+ to investigate wavepacket motion and fragmentation dynamics. The three transient ionization spectra of Na_8^+ in Fig. 21 are symmetric with respect to zero delay time, because pump and probe pulses had the same time duration and intensity. In order to determine the decay time constants we have analyzed the transient spectra with a sum of exponential decay functions. At 518 nm the best agreement between experimentation and simulation is

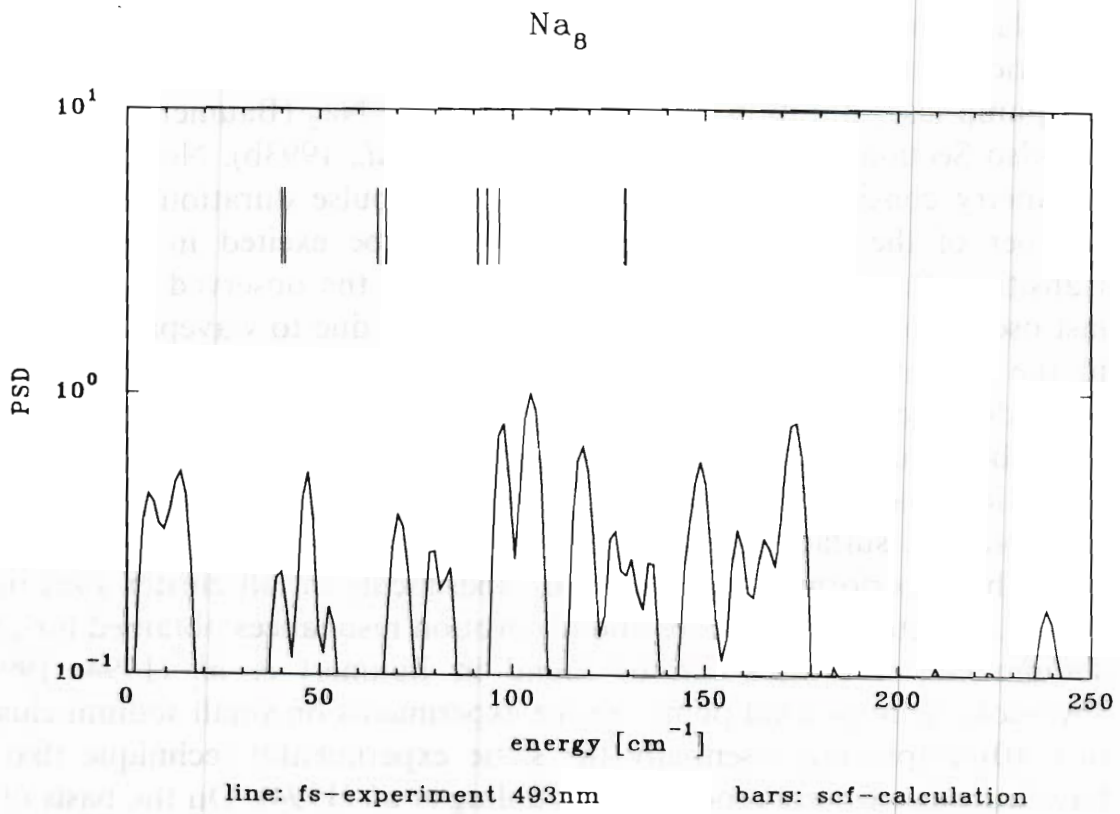

FIG. 22. Fast Fourier transformation of the transient Na_8^+ signal of Fig. 21 (at 493 nm). The obtained frequencies are in the range of the normal modes of small sodium clusters (see the text). The bars represent calculated frequencies of normal modes of the Na_8 ground state (Bonacic-Koutecky, 1994).

achieved by taking into account two contributions with time constants of 0.5 ps and of about 4 ps. For the transient spectrum obtained at 493 nm only a single exponential decay with a time constant of 0.45 ps describes the measured spectrum well. What is, however, clearly demonstrated by the different transient Na_8^+ spectra in Fig. 21 is that each absorption resonance has its own decay dynamics. Besides the observed decay of the signal there is also for each resonance an additional superimposed oscillatory structure. For the 518-nm resonance we find a regular oscillation with a time interval of about 160 fs, while at 493 nm at least two different series with time intervals of 360 and 270 fs are clearly seen. The transient spectrum of the 540-nm resonance is quite different from the two others. Here we observe a much slower dynamics with time constants of 0.8 and 2.8 ps. A fast Fourier transformation (FFT) of the time domain spectra at $\lambda = 493$ nm is displayed in Fig. 22 and shows frequencies corresponding to 360 and 270 fs and some additional frequencies in the range from 30 to 180 cm^{-1}. All these frequencies are in the range of the known vibrational eigenfrequencies of Na_3 and Na_4 as determined by ZEKE-photoelectron spectroscopy (Thalweiser *et al.*, 1993). The bars in Fig. 22 represent calculated normal mode frequencies of

the Na_8 ground state (Bonacic-Koutecky, 1994). Electronic ground state vibrational modes can be excited by stimulated emission pumping during the pump laser duration as has been shown in Na_2 (Baumert *et al.*, 1992c; see also Section III.D) and Na_3 (Baumert *et al.*, 1993b). Note that due to symmetry considerations and the ultrashort pulse duration only a small number of the $3N-6$ normal modes could be excited in an electronic transition. Based on this reasoning we believe the observed superimposed fast oscillations in the decay measurements are due to wavepacket motions in the potential surfaces of these metal clusters. The strong wavelength dependence of the decay time constants and the wavepacket motions are much better understood when taking into account molecular structures and excitations rather than considering Na_8 a metal sphere with delocalized electrons and surface plasmon-type excitations.

We have performed time-resolved experiments on all cluster sizes up to $n = 21$. Selected decay curves and absorption resonances obtained for other sodium cluster masses can be found in Baumert *et al.* (1994a, 1994b). Two-color femtosecond pump–probe experiments on small sodium clusters ($n \leqslant 10$) employing essentially the same experimental technique that we have introduced were reported by Kühling *et al.* (1994). On the basis of the number of observed cluster absorption resonances, their different energies and bandwidths, and their different decay patterns, we conclude that at least for cluster sizes Na_n with $n \leqslant 21$ molecular excitations and properties prevail over collective excitations and surface plasmon-like properties.

D. Experiments with Mercury Clusters and Fullerenes

In this section we will highlight experiments conducted on mercury clusters and fullerenes in which interesting ionization and fragmentation processes are observed in high-laser-intensity femtosecond single-pulse and pump–probe experiments.

1. Mercury Clusters

Clusters form a new class of materials, which often exhibit unexpected properties. A very interesting situation arises with mercury clusters. The mercury atom has a $5d^{10}6s^2np^0$ closed-shell electronic configuration with an ionization potential of 10.4 eV. Diatomic Hg_2 and other small mercury clusters are predominantly van der Waals-bound systems. However, the electronic structure changes strongly with increasing cluster size and finally converges toward the bulk, where the $6s$ and $6p$ bands overlap, giving mercury its metallic properties. This means that for the divalent Hg_n cluster a size-dependent transition from van der Waals to covalent and metallic

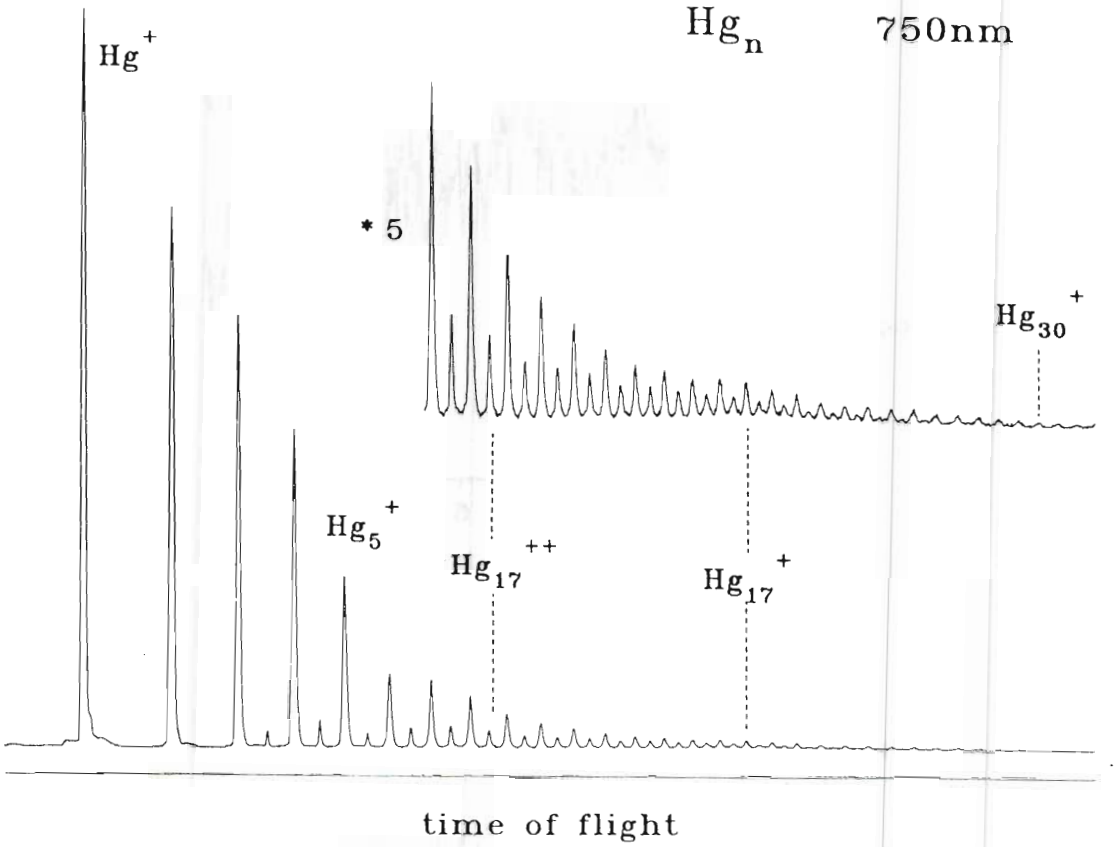

FIG. 23. Time-of-flight mass spectrum of singly and doubly charged mercury cluster ions.

binding exists. Therefore mercury provides the ideal system to study the size-dependent nonmetal–metal transition. For the neutral mercury cluster the ionization potentials are reasonably well known (Rademann *et al.*, 1987), but other optical properties are practically unknown. The situation is much better for singly and doubly ionized Hg_n clusters with the reported ionization potentials and optical absorption spectra (Haberland *et al.*, 1993).

Here we report the first studies of multiphoton ionization and fragmentation of mercury clusters in the femtosecond time domain. We observe the prompt formation of singly and doubly charged cluster ions and measure directly the decay of parent ions due to photofragmentation, together with the subsequent growth of daughter species. Furthermore we observe size-selected ion intensity oscillations in pump–probe measurements, indicating wave packet dynamics in both singly and doubly charged clusters. For these experiments we have used the Ti:sapphire laser, generating a train of light pulses 20–70 fs in duration. The pulses are amplified, compressed, and delayed to form a sequence of pump–probe pairs (see Fig. 3). TOF spectrometry determines the mass of the cluster ion and the initial kinetic energy of the ionic fragments.

Figure 23 shows a TOF mass spectrum of singly and doubly charged Hg_n cluster ions produced by 30-fs pulses at 750 nm. The most striking features of the spectrum are, first, that a multiphoton (6/12 photons) absorption

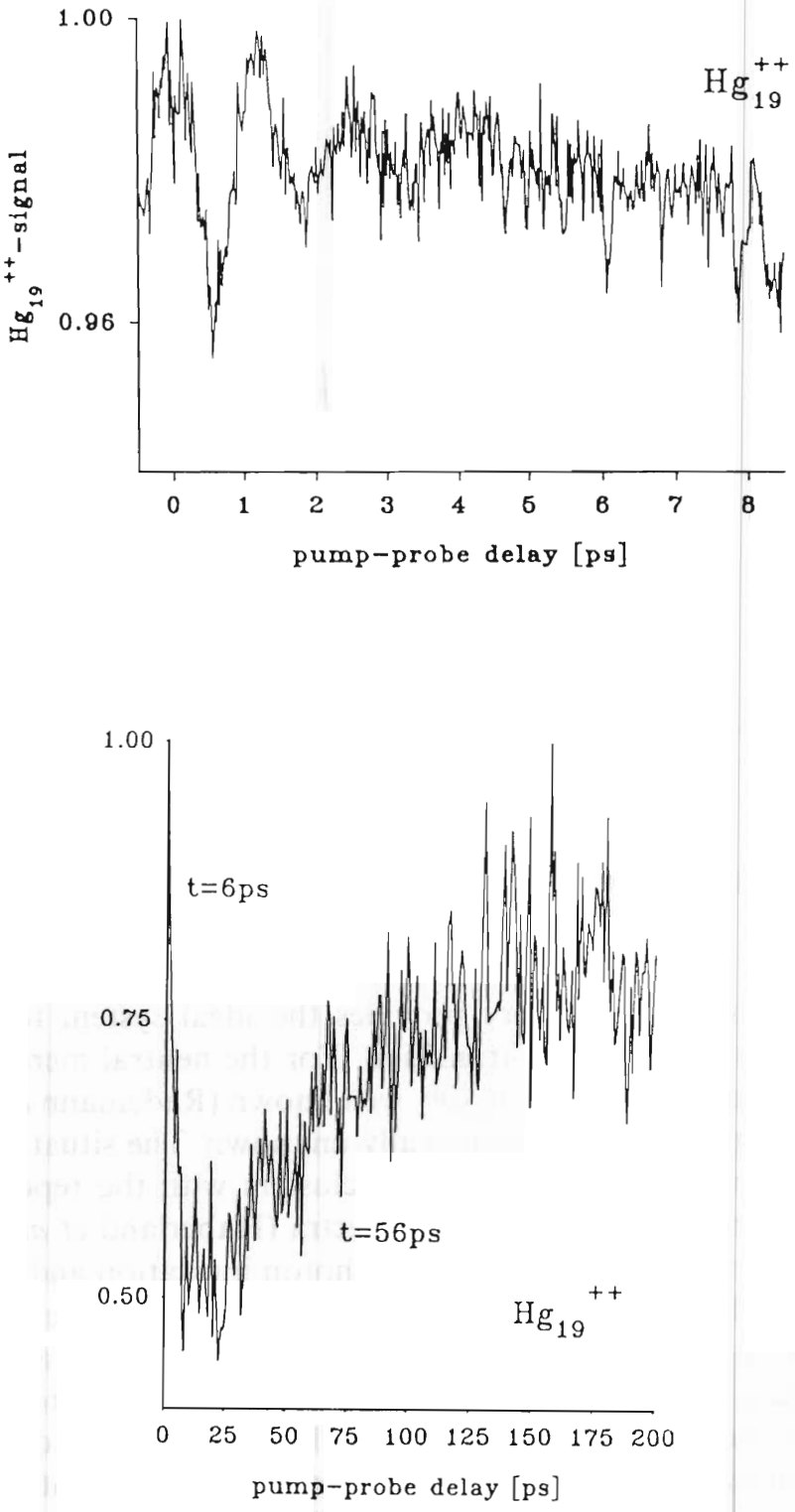

FIG. 24. Short-time dynamics (upper) and long-time dynamics (lower) of doubly charged Hg_{19} clusters.

forms singly and doubly ionized clusters and, second, that the intensity ratio between singly and doubly charged clusters of the same mass is in favor of the doubly charged species. Furthermore this ratio does not change for up to 10 times lower laser intensity, but the ratio does change strongly with wavelength.

A very surprising result of our time-resolved studies of size-selected neutral mercury clusters is shown in Fig. 24. The upper part of the figure details the first 8 ps of the pump–probe measurement of doubly charged Hg_{19}. The oscillatory behavior of this transient—indicating a wavepacket motion in a neutral cluster excited-state manifold—is seen in transient ionization spectra of singly and doubly charged clusters up to $n = 43$, for all $n \geqslant 5$.

The simplicity and similarity of the wavepacket motion over a broad range of cluster masses lead us to propose multiphoton absorption to a core Hg_2^* "chromophore" imbedded within and common to all the Hg_n neutral clusters examined in these experiments. The fact that blocking the probe pulse effectively quenches all ion signals and that the pump–probe spectrum with a weaker pump (or probe) is still symmetric with respect to $t = 0$ means that the pump pulse must excite a manifold of high-lying Rydberg states near but below the individual cluster ionization limit.

The lower part of Fig. 24 shows the long time dynamics of doubly charged Hg_{19} up to a 200-ps pump–probe delay time. Note the decrease in the signal at short delay times and the increase of the signal for long delay times. This type of transient was seen in time-resolved experiments on $I_2^-(CO_2)_n$ clusters in the Lineberger group (Papanikolas *et al.*, 1993) and in I_2Ar_n in the Zewail group (Potter *et al.*, 1992b; Lienau *et al.*, 1993) and is attributed to the cage effect, i.e., recombination induced by a surrounding solvent shell.

From the transient ionization spectra of singly and doubly charged mercury clusters it is clear that a maximum ion signal is observed for both species at precisely zero delay time. Note that this—together with the identical transients (0–8 ps) for singly and doubly charged clusters—suggests that double ionization occurs directly through a transition from the neutral to the doubly charged manifold and not via the singly ionized continuum as it is observed in many high-laser-field experiments with atoms and molecules. The observation that the ratio of observed singly and doubly charged clusters of the same mass is independent with laser intensity for at least a factor of 10 (as noted before) supports this interpretation.

2. *Fullerenes*

The ultrafast dynamics of isolated fullerenes C_{60} and C_{70} have been investigated in a molecular beam employing ion and electron TOF spectrometry in combination with femtosecond pump–probe laser techniques. Femtosecond pulses are generated in the CPM laser, amplified in bow ties and Bethune cells, and time delayed in a Michelson arrangement as described in Section II.

Multiphoton ionization with 620- and 310-nm femtosecond laser pulses shows no sign of delayed ionization. With nanosecond laser pulses, multiphoton ionization of fullerenes leads to microsecond-delayed ionization,

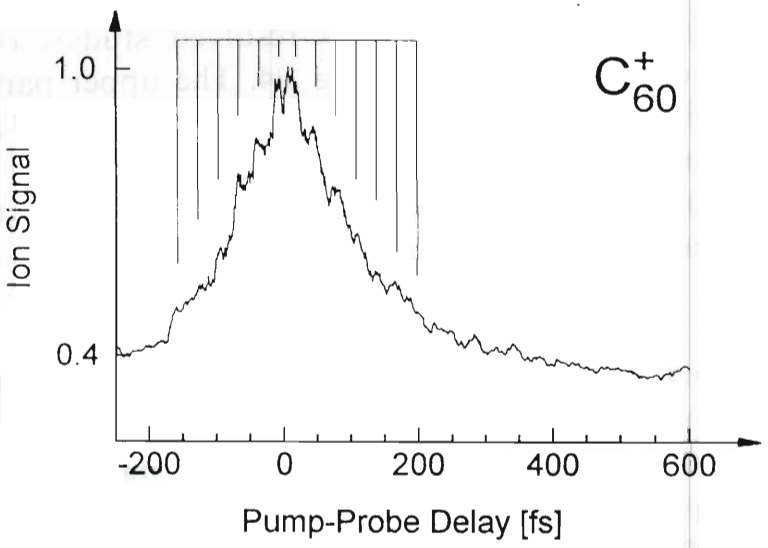

FIG. 25. Transient ionization signal of C_{60} obtained with 620-nm femtosecond pump and probe pulses. The ultrafast decay of the intermediate resonance is modulated by a 30-fs oscillatory structure.

often explained within a model of thermionic electron emission (Campbell *et al.*, 1991; Wurz and Lykke, 1991).

The transient ionization spectra of C_{60} and C_{70} for (2 + 2) photoionization at 620 nm with 60-fs pulses show a very fast decay. In the case of C_{60}—the actual measurement is shown in Fig. 25—it can be represented by a double exponential decay with about 100-fs and 3-ps time constants, while for C_{70} only the fast decay of about 100 fs is observed. Superimposed on the C_{60} decay curve is a 30-fs oscillatory structure. A Fourier transformation of the C_{60} transient gives frequencies in a range of 500 to 1600 cm^{-1} with a dominant peak at 1128 cm^{-1}. Frequencies in that range have been seen, for instance, in Fourier transform infrared (FTIR) C_{60} thin-film absorption spectra (Meilunas *et al.*, 1991).

The TOF ion spectrum obtained at the threshold of multiphoton ionization of the fullerenes contains only C_{60}^+ and C_{70}^+. For laser intensities of 10^{12} W/cm^2 and higher, doubly and triply charged fullerenes and fragments are observed. The corresponding electron spectra show in both cases only one broad peak. However, it is surprising that the relative signal strengths of the singly, doubly, and triply charged species do not change with increasing laser intensity. This is clearly in contradiction to the conventionally discussed stepwise excitation process. We believe this result indicates a new not yet fully understood ionization mechanism in high laser fields. Moreover we observe only even-numbered neutral and multiple ($n = 1, 2, 3$) charged fragments like C_{58}^{n+}, C_{56}^{n+}, ..., C_{42}^{n+} from C_{60} for both 620- and 310-nm radiation. The measured initial kinetic energy release of the fragments indicates a fission of the parent fullerene rather than a sequential loss, which is reported to be the major channel in nanosecond experiments.

V. Conclusions

The real-time dynamics of multiphoton ionization and fragmentation of sodium and mercury molecules and clusters and of fullerenes have been studied in molecular beam experiments employing femtosecond pump–probe techniques and ion and electron spectroscopy.

Sodium with one valence electron per atom is an experimentally and theoretically very attractive system. Femtosecond time-resolved multiphoton ionization of sodium molecules reveals unexpected features in the dynamics of the absorption of several photons:

In Na_2 a second major REMPI process involving stepwise excitation of *two* electrons and subsequent electronic autoionization is observed in addition to the direct *one*-electron photoionization process. The femtosecond pump–probe technique demonstrates the possibility of controlling reactions by controlling the duration of propagation of a wavepacket on an excited electronic surface, as the ratio of Na_2^+ vs Na^+ varies by more than 100% as a function of pump–probe delay time.

The contribution of the one-electron REMPI process versus the two-electron REMPI process to the total ion yield varies strongly with the applied laser field strength. This can be understood by coherent coupling of the electronic states participating in these REMPI processes, leading to laser-intensity-dependent Rabi-type population switching between these states. At high laser intensities a wavepacket in the electronic ground state of Na_2 is created by stimulated emission pumping during the pump pulse duration. The $2\,^1\Sigma_u^+$ double minimum state of Na_2 is given as an example of how to perform frequency spectroscopy through time domain measurements.

Cluster physics bridge the gap between molecular and solid-state physics. Cluster size-dependent studies of physical properties such as absorption resonances, lifetimes, and decay channels have been performed with tunable, ultrashort light pulses. A major result of our femtosecond experiments is that the conventional view of the optical response of a metal cluster, e.g., the absorption, ionization, and decay processes as well as the corresponding time scales, had to be changed. Our results clearly show that for cluster sizes of Na_n with $n \leqslant 21$, the molecular structure, excitations, and properties prevail over collective excitations and surface plasmon-like properties. It is, however, obvious that for even larger clusters the optical response must finally be dominated by collective interactions.

The preliminary analysis of the time-resolved mercury experiments gives astonishing results. First, the observation of singly and doubly ionized clusters in direct multiphoton ionization transitions and, second, an almost identical vibrational wavepacket motion in both singly and doubly charged clusters up to $n = 43$ are very surprising. Probably an Hg_2^* chromophore

imbedded within and common to all Hg_n neutral clusters carries the oscillator strength and determines the short-time wavepacket dynamics.

In multiphoton ionization of isolated fullerenes with high-intensity femtosecond laser pulses singly, doubly, and triply charged fullerenes and fragments are observed. The relative signal strength of the different charged species does not change with increasing laser intensity. This cannot be explained within the conventionally discussed stepwise excitation process. The real-time studies of the dynamics of ionization and fragmentation with femtosecond time resolution open up new and very exciting fields in molecular and cluster physics and yield results which in many cases are not accessible in nanosecond or picosecond laser experiments.

Acknowledgments

We gratefully acknowledge discussions with V. Engel and C. Meier and in particular the contributions of A. Assion, B. Bühler, M. Grosser, B. Lang, D. Schulz, V. Seyfried, R. Thalweiser, V. Weiss, and E. Wiedenmann to the various experiments. This work has been supported by the Deutsche Forschungsgemeinschaft through the Sonderforschungsbereich 276 "Korrelierte Dynamik hochangeregter atomarer und molekularer Systeme" in Freiburg.

References

Asaki, M. T., Huang, C.-P., Garvey, D., Zhou, J., Kapteyn, H. C., and Murnane, M. M. (1993). *Opt. Lett.* **18**, 977.

Averbukh, I. S., and Perelman, N. F. (1989). *Phys. Lett. A* **139**, 449.

Baumert, T., and Gerber, G. (1994). *Is. J. Chem.* **34**, 103.

Baumert, T., Bühler, B., Thalweiser, R., and Gerbert, G. (1990). *Phys. Rev. Lett.* **64**, 733.

Baumert, T., Grosser, M., Thalweiser, R., and Gerber, G. (1991a). *Phys. Rev. Lett.* **67**, 3753.

Baumert, T., Bühler, B., Grosser, M., Thalweiser, R., Weiss, V., Wiedenmann, E., and Gerber, G. (1991b). *J. Phys. Chem.* **95**, 8103.

Baumert, T., Engel, V., Röttgermann, C., Strunz, W. T., and Gerber, G. (1992a). *Chem. Phys. Lett.* **191**, 639.

Baumert, T., Röttgermann, C., Rothenfußer, C., Thalweiser, R., Weiss, V., and Gerber, G. (1992b). *Phys. Rev. Lett.* **69**, 1512.

Baumert, T., Engel, V., Meier, C., and Gerber, G. (1992c). *Chem. Phys. Lett.* **200**, 488.

Baumert, T., Pedersen, S., and Zewail, A. H. (1993a). *J. Phys. Chem.* **97**, 12447.

Baumert, T., Thalweiser, R., and Gerber, G. (1993b). *Chem. Phys. Lett.* **209**, 29.

Baumert, T., Thalweiser, R., Weiss, V., Wiedenmann, E., and Gerber, G. (1994a). In *Femtosecond Reaction Dynamics* (Wiersma, D. A., ed.), p. 29, North-Holland Publ., Amsterdam.

Baumert, T., Thalweiser, R., Weiss, V., and Gerber, G. (1994b). In *Femtosecond Chemistry* (Manz, J., and Wöste, L., eds.), p. 397, Verlag Chemie, Berlin.

Bonacic-Koutecky, V. (1994). Private communication.

Bonacic-Koutecky, V., Fantucci, P., and Koutecky, J. (1990a). *J. Chem. Phys.* **93**, 3802.

Bonacic-Koutecky, V., Kappes, M. M., Fantucci, P., and Koutecky, J. (1990b). *Chem. Phys. Lett.* **170**, 26.
Bonacic-Koutecky, V., Pittner, J., Scheuch, C., Guest, M. F., and Koutecky, J. (1992). *J. Chem. Phys.* **96**, 7938.
Bordas, C., Labastie, P., Chevaleyre, J., and Broyer, M. (1989). *Chem. Phys.* **129**, 21.
Bowman, R. M., Dantus, M., and Zewail, A. H. (1989). *Chem. Phys. Lett.* **161**, 297.
Brack, M. (1993). *Rev. Mod. Phys.* **65**, 677.
Bréchignac, C., Cahuzac, P., Roux, J. P., Pavolini, D., and Spiegelmann, F. (1987). *J. Chem. Phys.* **87**, 5694.
Broyer, M., Delacrétaz, G., Labastie, P., Whetten, R. L., Wolf, J. P., and Wöste, L. (1986a). *Z. Phys. D* **3**, 131.
Broyer, M., Delacrétaz, G., Labastie, P., Wolf, J., and Wöste, L. (1986b). *Phys. Rev. Lett.* **57**, 185.
Broyer, M., Delacrétaz, G., Labastie, P., Wolf, J. P., and Wöste, L. (1987). *J. Phys. Chem.* **91**, 2626.
Broyer, M., Delacrétaz, G., Guoquan, N., Wolf, J. P., and Wöste, L. (1988). *Chem. Phys. Lett.* **145**, 232.
Burkhardt, C. E., Barver, W. P., and Leventhal, J. J. (1985). *Phys. Rev. A* **31**, 505.
Campbell, E. E. B., Ulmer, G., and Hertel, I. V. (1991). *Phys. Rev. Lett.* **67**, 1986.
Clemenger, K. (1985). *Phys. Rev. B* 32, 1359.
Cooper, D. L., Barrow, R. F., Vergès, J., Effantin, C., and d'Incan, J. (1984). *Can. J. Phys.* **63**, 1543.
de Heer, W. A. (1993). *Rev. Mod. Phys.* **65**, 611.
Delacrétaz, G., and Wöste, L. (1985). *Chem. Phys. Lett.* **120**, 342.
Eckardt, W. (1984a). *Phys. Rev. B* **29**, 1558.
Eckardt, W. (1984b). *Phys. Rev. Lett.* **52**, 1925.
Eckardt, W., and Penzar, Z. (1988). *Phys. Rev. B* **38**, 4273.
Eckardt, W., and Penzar, Z. (1991). *Phys. Rev. B* **43**, 1322.
Engel, V. (1991a). *Comp. Phys. Commun.* **63**, 228.
Engel, V. (1991b). *Chem. Phys. Lett.* **178**, 130.
Engel, V., Baumert, T., Meier, C., and Gerber, G. (1993). *Z. Phys. D* **28**, 37.
Fork, R. L., Greene, B. I., and Shank, C. V. (1981). *Appl. Phys. Lett.* **38**, 671.
Fragnito, H. L., Bigot, J.-Y., Becker, P. C., and Shank, C. V. (1989). *Chem. Phys. Lett.* **160**, 101.
Gerber, G., and Möller, R. (1985). *Chem. Phys. Lett.* **113**, 546.
Gruebele, M., Roberts, G., Dantus, M., Bowman, R. M., and Zewail, A. H. (1990). *Chem. Phys. Lett.* **166**, 459.
Haberland, H., von Issendorf, B., Yufeng, J., Kolar, T., and Thanner, G. (1993). *Z. Phys. D.* **26**, 8.
Haugstätter, R., Goerke, A., and Hertel, I. V. (1988). *Z. Phys. D* **9**, 153.
Heist, P., Rudolph, W., and Wilhelmi, B. (1990). *Exp. Tech. Phys.* **38**, 163.
Ippen, E. P., and Shank, C. V. (1977). In *Ultrafast Light Pulses* (Shapiro, S. L., ed.), Topics in Applied Physics, Vol. 18, p. 83, Springer-Verlag, Berlin.
Jacobovitz, G. R., Brito Cruz, C. H., and Scarparo, M. A. (1986). *Opt. Commun.* **57**, 133.
Janssen, M. H. M., Bowman, R. M., and Zewail, A. H. (1990). *Chem. Phys. Lett.* **172**, 99.
Jeung, G. (1983). *J. Phys. B* **16**, 4289.
Kappes, M. M., Schär, M., Röthlisberger, U., Yeretzin, C., and Schumacher, E. (1988). *Chem. Phys. Lett.* **143**, 251.
Keller, J., and Weiner, J. (1984). *Phys. Rev. A* **30**, 213.
Knox, W. H. (1988). *IEEE J. Quantum Electron.* **QE-18**, 101.
Kogelnik, H., and Li, T. (1966). *Appl. Opt.* **5**, 1550.
Koskinen, M., Manninen, M., and Lipas, P. O. (1994). *Phys. Rev. B* **49**, 8418.
Kühling, H., Kobe, K., Rutz, S., Schreiber, E., and Wöste, L. (1994). *J. Phys. Chem.* **98**, 6679.
Kulander, K. C., and Heller, E. J. (1978). *J. Chem. Phys.* **69**, 2439.
Kusch, P., and Hessel, M. M. (1978). *J. Chem. Phys.* **68**, 2591.

Li, K. K. (1982). *Appl. Opt.* **21**, 967.
Lienau, C., Williamson, J. C., and Zewail, A. H. (1993). *Chem. Phys. Lett.* **213**, 289.
Meier, C. (1992). Diplomarbeit, Univ. Freiburg.
Meier, C., and Engel, V. (1994a). *J. Chem. Phys.* **101**, 2673.
Meier, C., and Engel, V. (1994b). Private communication.
Meier, C., and Engel, V. (1994c). *Phys. Rev. Lett.* **73**, 3207.
Meilunas, R., Chang, R. P. H., Liu, S., Jensen, M., and Kappes, M. M. (1991). *J. Appl. Phys.* **70**, 5128.
Meyer, W. (1992). Private communication.
Mie, G. (1908). *Ann. Phys. (Leipzig)* **25**, 377.
Müller-Dethlefs, K., Sander, M., and Schlag, E. W. (1984). *Z. Naturforsch. A* **39A**, 1089.
Mulliken, R. S. (1971). *J. Chem. Phys.* **55**, 309.
New, G. (1974). *IEEE J. Quantum Electron.* **QE-10**, 115.
Noordam, L. D., Joosen, W., Broers, B., ten Wolde, A., Lagendijk, A., Van Linden van den Heuvell, H. B., and Muller, H. G. (1991). *Opt. Commun.* **85**, 331.
Ogorzalek Loo, R., Hall, G. E., Haerri, H.-P., and Houston, P. L. (1988). *J. Phys. Chem.* **92**, 5.
Papanikolas, J. M., Vorsa, V., Nadal, E. M., Campagnola, P. J., Buchenau, H. K., and Lineberger, W. C. (1993). *J. Chem. Phys.* **99**, 8733.
Penzar, Z., and Eckardt, W. (1990). *Z. Phys. D* **17**, 69.
Potter, E. D., Herek, J. L., Pedersen, S., Liu, Q., and Zewail, A. H. (1992a). *Nature (London)* **355**, 66.
Potter, E. D., Liu, Q., and Zewail, A. H. (1992b). *Chem. Phys. Lett.* **200**, 605.
Rademann, K., Kaiser, B., Even, U., and Hensel, F. (1987). *Phys. Rev. Lett.* **59**, 2319.
Rigrod, W. W. (1965). *Bell Syst. Tech. J.* May, p. 907.
Rubio, A., Balbas, L. C., and Alonso, J. A. (1992). *Phys. Rev. B* **46**, 4891.
Schrödinger, E. (1926). *Naturwissenschaften* **14**, 664.
Selby, K., Vollmer, M., Masui, J., Kresin, V., de Heer, W. A., and Knight, W. D. (1989). *Phys. Rev. B* **40**, 5417.
Simon, J. D. (1989). *Rev. Sci. Instrum.* **60**, 3597.
Squier, J., Korn, G., Mourou, G., Vaillancourt, G., and Bouvier, M. (1993). *Opt. Lett.* **18**, 625.
Stingl, A. (1994). *Adriat. Res. Conf. Ultrafast Phenom. Appl. Trieste* (lecture).
Stingl, A., Spielmann, C., and Krausz, F. (1994). *Opt. Lett.* **19**, 204.
Strickland, D., and Mourou, G. (1985). *Opt. Commun.* **56**, 219.
Tannor, D. J., Kosloff, R., and Rice, S. A. (1986). *J. Chem. Phys.* **85**, 5805.
Taylor, A. J., Jones, K. M., and Schawlow, A. L. (1983). *J. Opt. Soc. Am.* **73**, 994.
ten Wilde, A., Noordam, L. D., Muller, H. G., and van Linden van den Heuvell, H. B. (1989). In *Fundamentals of Laser Interaction II* (F. Ehlotzky, ed.), Lecture Notes in Physics, No. 339, p. 194, Springer-Verlag, Berlin.
Thalweiser, R. (1992). Thesis, Univ. Freiburg.
Thalweiser, R., Vogler, S., and Gerber, G. (1993). *SPIE Proc.* **1858**, 196.
Ultrafast Phenomena IX (1994). (Knox, W., Barbara, P., Mourou, G. A., and Zewail, A. H., eds.), Springer Series in Chemical Physics, Vol. 60, Springer-Verlag, Berlin.
Valance, A., and Nguyen, Tuan, Q. (1982). *J. Phys. B* **15**, 17.
Valdmanis, J. A., and Fork, R. L. (1986). *IEEE J. Quantum Electron.* **QE-22**, 112.
Vergès, J., Effantin, C., d'Incan, J., Cooper, D. L., and Barrow, R. F. (1984). *Phys. Rev. Lett.* **53**, 46.
Wang, C. R. C., Pollack, S., Cameron, D., and Kappes, M. M. (1990). *J. Chem. Phys.* **93**, 3787.
Wang, C. R. C., Pollack, S., Dahlseid, T. A., Koretsky, G. M., and Kappes, M. M. (1992). *J. Chem. Phys.* **96**, 7931.
Warren, W. S., Rabitz, H., and Dahleh, M. (1993). *Science* **259**, 1581.
Wiley, W. C., and McLaren, I. H. (1955). *Rev. Sci. Instrum.* **26**, 1150.
Wurz, P., and Lykke, K. R. (1991). *J. Chem. Phys.* **95**, 7008.
Yeazell, J. A., Mallalieu, M., and Stroud, C. R., Jr. (1990). *Phys. Rev. Lett.* **64**, 2007.